ACS MATERIALS LETTERS

www.acsmaterialsletters.org

PERSPECTIVE

Efficient Lone-Pair-Driven Luminescence: Structure–Property Relationships in Emissive $5s^2$ Metal Halides

Kyle M. McCall, Viktoriia Morad, Bogdan M. Benin, and Maksym V. Kovalenko*

Cite This: *ACS Materials Lett.* 2020, 2, 1218–1232

Read Online

ACCESS | Metrics & More | Article Recommendations

ABSTRACT: **Low-dimensional metal halides have been the focus of intense investigations in recent years following the success of hybrid lead halide perovskites as optoelectronic materials. In particular, the light emission of low-dimensional halides based on the $5s^2$ cations Sn^{2+} and Sb^{3+} has found utility in a variety of applications complementary to those of the three-dimensional halide perovskites because of its unusual properties such as broadband character and highly temperature-dependent lifetime. These properties derive from the exceptional chemistry of the $5s^2$ lone pair, but the terminology and explanations given for such emission vary widely, hampering efforts to build a cohesive understanding of these materials that would lead to the development of efficient optoelectronic devices. In this Perspective, we provide a structural overview of these materials with a focus on the dynamics driven by the stereoactivity of the $5s^2$ lone pair to identify the structural features that enable strong emission. We unite the different theoretical models that have been able to explain the success of these bright $5s^2$ emission centers into a cohesive framework, which is then applied to the array of compounds recently developed by our group and other researchers, demonstrating its utility and generating a holistic picture of the field from the point of view of a materials chemist. We highlight those state-of-the-art materials and applications that demonstrate the unique capabilities of these versatile emissive centers and identify promising future directions in the field of low-dimensional $5s^2$ metal halides.**

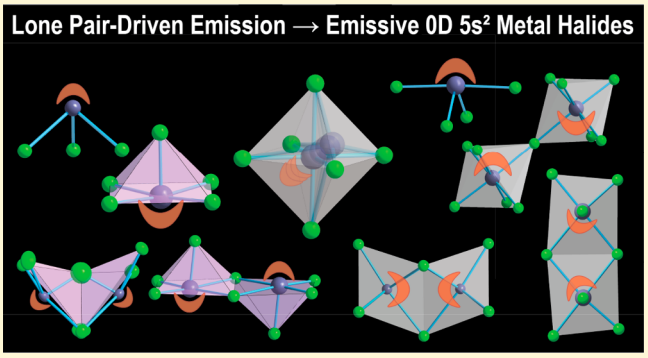

The rise of lead halide perovskites $APbX_3$ (with A^+ being a large cation and X^- a halide) as exceptional optoelectronic compounds has kindled immense interest in related main-group metal halides over the past decade.[1−4] These are unique semiconductors because of the mix of covalent bonding in the inorganic $[PbX_{6/2}]^-$ framework and ionic bonding to the A cation, yielding a dynamic structure that allows for local polar fluctuations,[5] electron−phonon coupling,[6] and the formation of large polarons to screen charge carriers.[7] The remarkable optoelectronic features of these three-dimensional (3D) materials include long charge carrier diffusion lengths and lifetimes[8,9] as well as bright, narrow emission in nanocrystalline form,[10] properties that are enhanced drastically by their defect-tolerant nature. This defect tolerance is based on the antibonding properties of the $6s^2$ lone pair of the heavy metal Pb^{2+} coupled to halide p orbitals, which forces defects to be very shallow or even lie outside the band gap.[3,11]

To replicate or improve upon the lead halide perovskites, the community turned to main-group metals with ns^2 lone pairs, primarily Sn^{2+}, Sb^{3+}, and Bi^{3+}.[12] Spurred by solar cell research, which requires higher dimensionalities and the heavier halogens to maintain the low band gaps needed to provide efficient solar absorption, initial efforts began with $CsSnI_3$,[13] $Cs_3M_2I_9$ (M = Sb, Bi),[14,15] and the quasi-two-dimensional (2D) Ruddlesden–Popper perovskites.[16] The shift to lower dimensionality permitted a great deal of structural flexibility, and a plethora of metal halides soon followed, from 3D double perovskites $A_2M^+M^{3+}X_6$ (M^+ = Ag, In, Tl; M^{3+} = Sb, In, Bi),[17] to fully zero-dimensional (0D) hybrid systems with large cations completely isolating square-pyramidal[18] or octahedral[19] metal halide units. Even considering only octahedral metal halides, the myriad

Received: May 22, 2020
Accepted: August 4, 2020
Published: August 4, 2020

https://dx.doi.org/10.1021/acsmaterialslett.0c00211
ACS Materials Lett. 2020, 2, 1218–1232

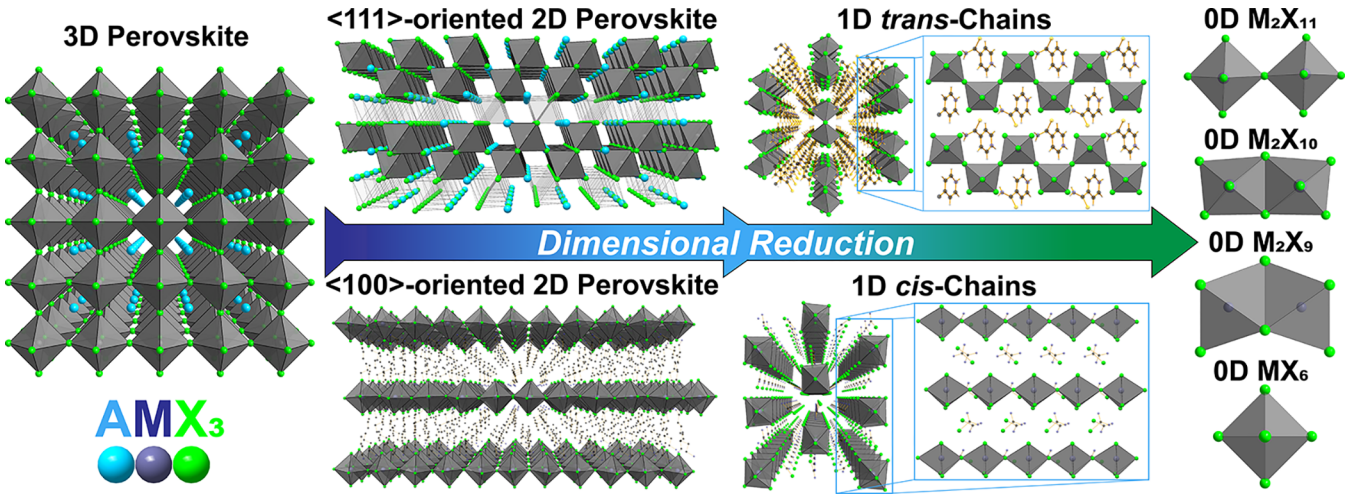

Figure 1. Structural versatility of octahedral metal halides: dimensional reduction of the aristotypical AMX_3 3D perovskite to low-dimensional metal halides.

choices of compatible cations (organic and inorganic) generate an impressive array of structure types (Figure 1), described further below.

The varied dimensionalities of metal halide perovskites give rise to a plethora of different properties deriving from the disruption of the 3D perovskite framework. For example, in 2D hybrid perovskites, the alternating organic−inorganic layers lead to anisotropic charge transport[20] and dramatic enhancements in the exciton binding energy due to dielectric confinement.[21] Compositional tuning is similarly critical. For example, the importance of electronic dimensionality has been demonstrated in the double perovskites, which often behave similarly to 0D systems despite their 3D crystal structure.[22,23]

The varied dimensionalities of metal halide perovskites give rise to a plethora of different properties deriving from the disruption of the 3D perovskite framework.

The structural confinement found in low-dimensional metal halides generates vastly different properties compared with their 3D counterparts, in particular with regard to the mechanism for light emission. Low dimensionality tends to favor the formation of self-trapped excitons (STEs),[24,25] the recombination of which yields broadband photoluminescence (PL) with generally longer lifetimes.[25−27] The emission of related compounds has also been interpreted using the frameworks of ion emission and atomic orbital theory.[28−31] Recent work has begun to realize the potential of these low-dimensional metal halides for a variety of applications complementary to the solar cells and narrow emitters of the 3D halide perovskites, namely, in solid-state lighting,[18,32] X-ray scintillation,[33,34] and remote thermometry.[35] Of these, the highest photoluminescence quantum yields (PLQYs) at room temperature (RT) have been based on Sn^{2+} or Sb^{3+} cations containing the active $5s^2$ lone pair.[19,34,36−40]

In this Perspective, we seek to provide insight into the structure−property relationships that dictate the performance of low-dimensional, emissive $5s^2$ materials. While the focus here is on 0D compounds, there is a rich chemistry of these materials that has not been fully explored for light emission, and thus, we begin with a structural overview. In particular, we highlight the stereoactive effects of the $5s^2$ lone pair, which generates the appropriate atomic environments for such emission, and unify the language used to describe this emission by considering the terminologies of ion emission, the atomic orbital approach, and the self-trapped exciton model. We believe that this burgeoning field will benefit from a common mechanistic understanding and a summary of the available structure types that exhibit broadband emission.

DIMENSIONALITY AND EMISSION IN OCTAHEDRAL METAL HALIDES

Here a brief introduction to dimensional reduction of metal halides is given through the series of perovskite-derivative structures based largely on corner-connected octahedral metal cations (Figure 1). We must mention that a variety of other non-perovskite polytypes exist, such as the face-shared octahedra of hexagonal perovskites[41] or entirely non-octahedral structures, with similar diversity of dimensionalities and properties.[36,42−45] The aristotypical 3D perovskite exhibits a cubic structure, with lower-symmetry structures derived from octahedral tilts[46] in cases with a non-ideal Goldschmidt tolerance factor.[1] Halide perovskites exhibit band-edge emission at RT with high internal PLQYs and efficient photon recycling,[47,48] but self-absorption leads to weak PLQYs in bulk, so isolation as nanocrystals is needed to achieve emission with high external PLQYs.[4,10]

The shift to 2D structures already leads to a variety of different structure types, the properties of which are dictated by the direction along which the perovskite framework is cut.[49,50] ⟨100⟩ 2D perovskites consist of flat slabs of octahedral layers interspersed with layers of large organic cations, yielding the Ruddlesden−Popper or Dion−Jacobsen perovskites (Figure 1).[2,16,51] The shape of the perovskite framework is maintained with such flat sheets, so the ⟨100⟩ 2D materials somewhat resemble their 3D counterparts with high absorption coefficients, dispersive band structures within the inorganic layer, and good solar cell efficiencies.[20,52,53] However, the introduction of large interlayer organic cations interrupts the covalent perovskite framework, generating a quantum well structure with anisotropic optical and electronic properties and extremely high exciton binding energies due to dielectric confinement.[21] These large binding energies stabilize free

https://dx.doi.org/10.1021/acsmaterialslett.0c00211
ACS Materials Lett. 2020, 2, 1218−1232

excitons at room temperature, causing bulk ⟨100⟩ 2D perovskites to emit more efficiently at room temperature.[54] Broad emission from STEs is common at low temperatures but requires structural distortion of the Pb−X−Pb angle to manifest at room temperature,[26] so free exciton emission is most common in the ⟨100⟩ 2D perovskites.

The ⟨110⟩-type 2D perovskites possess further anisotropy, as corner-sharing occurs in a straight line along one direction while the other direction has zig-zag chains that disrupt charge transport within the inorganic layer, providing further confinement.[55,56] In some sense, the ⟨110⟩ 2D perovskites share more similarities to one-dimensional (1D) perovskites than to their ⟨100⟩ or 3D counterparts, and accordingly, the emission properties of these materials are drastically different, with the manifestation of RT STE emission in ⟨110⟩ perovskites.[26,57,58] This class represents an edge case in this regard, as it includes several ⟨110⟩ compositions exhibiting both free exciton and STE emission.[26,56]

2D defect perovskites formed from trivalent cations (e.g., Sb^{3+} or Bi^{3+}) must balance the excess charge on the M site with one-third occupancy of vacancies; this yields the formula $A_3M_2\square X_9$ (where □ represents a vacancy) and forms bilayers cut along the ⟨111⟩ direction of the 3D perovskite (Figure 1).[59,60] It should be noted that the ⟨111⟩ direction of the 3D perovskite corresponds to the R symmetry point of the Brillioun zone, where the band edge states lie, and thus, the 2D defect perovskite most effectively breaks up the 3D perovskite. Furthermore, while this structure maintains 2D hexagonal symmetry within the octahedral layer, it is further removed from the 3D perovskite than the ⟨100⟩ or ⟨110⟩ 2D perovskites because no straight lines connect more than two octahedra.[61] Accordingly, these compounds exhibit STEs and relatively poor charge transport properties compared with either 3D or ⟨100⟩ 2D perovskites.[14,61,62] For further information on 2D perovskites, we refer the reader to recent reviews that describe these compounds in greater detail.[50,51]

Further reducing the dimensionality to 1D compounds begets wholly different properties compared with the 3D perovskites because of the limitation of orbital overlap to a single crystallographic axis. While there are a variety of corner-connected octahedral structures ranging from straight trans-connected chains to zigzag cis-connected chains (Figure 1)[63] and corrugated double chains,[64] their optical properties are relatively underexplored. The corrugated compounds $Cs_3M_2Cl_9$ (M = Sb, Bi) are known to be emissive at low temperatures only,[65] whereas efficient STE emission from 1D metal halides has been obtained from edge-shared double chains.[66]

0D metal halides possess fully isolated octahedral units, which can be bridged by inorganic cations as in Cs_4SnBr_6 or large organic cations as in $(C_4N_2H_{14}Br)_4SnBr_6$.[19,37] While corner-connected octahedra form many higher-dimensional frameworks, corner-connected 0D clusters are quite rare: no divalent cations exhibit such anions, while only seven compounds are known to exhibit the dimeric $[M_2X_{11}]^{5-}$ anion.[67]

Instead, 0D octahedral clusters tend toward edge-sharing or face-sharing octahedra to help reduce the total charge of the anion. For example, in Sb-based dimers the total charge on the anion decreases from −5 in corner-shared Sb_2Br_{11} to −4 in edge-shared Sb_2X_{10} and −3 in face-shared Sb_2X_9 (Figure 1). Such polynuclear clusters can contain as many as eight or 18 octahedra for trivalent and bivalent cations, respectively.[44,68] However, such clusters have not been extensively explored for their optical properties, and hence, the focus here is on the fully isolated 0D structures built of mononuclear emissive metal centers. The emission of fully 0D metal halides is based wholly on STEs and is most efficient for the fully isolated octahedra, especially with large organic cations.[19,37]

0D UNITS AND CHEMISTRY OF THE $5s^2$ LONE PAIR

In addition to octahedral units, ns^2 metal halides can form structures based on pyramidal MX_3 units, disphenoidal MX_4 units, and square-pyramidal MX_5 coordination (Figure 2),[31,43]

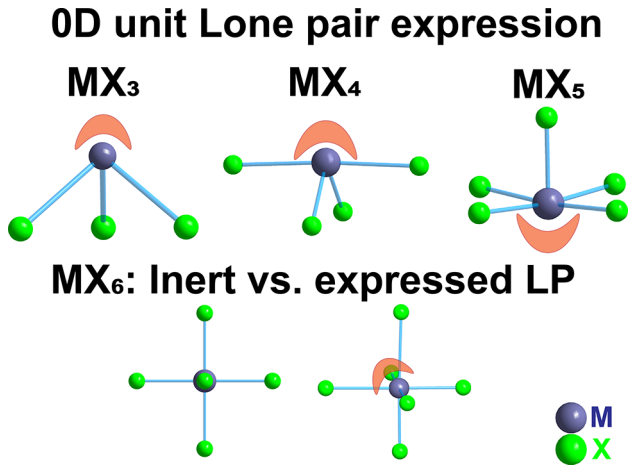

Figure 2. Atomic environments of 0D ns^2 metal halides, with the lone pair visualized in orange.

which can be built into polymeric frameworks and chains just as in the case of the octahedral metal halides.[43,69] The increasing structural diversity with reduced dimensionality is illustrated in Table 1 for $5s^2$-based metal halides (Sn^{2+}, Sb^{3+}), with archetypes

Table 1. Anionic $5s^2$ Metal Halide Structural Units

X/M	0D		1D		2D	
2.5					$[Sn_2X_5]_\infty^-$	70
3	$[SnX_3]^-$	71	$[SnX_3]_\infty^-$	41		
3.5	$[Sb_2X_7]^-$	72			$[Sn_2X_7]_\infty^{3-}$	73
4	$[SnX_4]^-$	34	$[SbX_4]_\infty^-$	75	$[SnX_4]_\infty^{2-}$	76
	$[Sb_2X_8]^{2-}$	74				
4.5	$[Sb_2X_9]^{3-}$	14			$[Sb_2X_9]_\infty^{3-}$	14
	$[Te_2X_9]^-$	77				
5	$[SbCl_5]^{3-}$	18	$[SnX_5]_\infty^{3-}$	81		
	$[Sn_2X_{10}]^{6-}$	78	$[SbX_5]_\infty^{2-}$	82		
	$[Sb_2X_{10}]^{4-}$	79	$[TeX_5]_\infty^-$	83		
	$[Te_2X_{10}]^{2-}$	80				
5.5	$[Sb_2X_{11}]^{5-}$	84				
6	$[SnX_6]^{4-}$	19				
	$[SbX_6]^{3-}$	85				
	$[TeX_6]^{2-}$	86				

**compounds with room-temperature emission shown in green

known to exhibit emission at room temperature marked in green. The coordinative flexibility of 0D units permits a wide range of structures, many of which possess emission at room temperature. It should be noted that the table is limited to dimeric units for clarity and that a variety of polynuclear 0D compounds exist beyond those listed.[43,44,87]

https://dx.doi.org/10.1021/acsmaterialslett.0c00211
ACS Materials Lett. 2020, 2, 1218−1232

The coordinative flexibility of 0D units permits a wide range of structures, many of which possess emission at room temperature.

Excited states play a critical role in the optoelectronic properties of metal halides, and in these 0D complexes the geometry is dictated by the outer-shell ns^2 lone pair electrons.[31] Hence, it is helpful to visualize the stereochemistry of the lone pair in each coordination environment, shown in orange in Figure 2. The lone pair induces a statically expressed distortion in these units, from the expected trigonal-planar to trigonal-pyramidal in MX_3 anions, tetragonal to disphenoidal in MX_4 anions, and trigonal-bipyramidal to square-pyramidal in MX_5.[31]

In contrast, the octahedral MX_6 anion can be found in either inert crystallographic environments, where the site symmetry is essentially cubic,[37,88] or in environments where the lone pair is expressed through a trigonal or tetragonal deformation.[19,85,89] Intriguingly, even the inert MX_6 octahedron exhibits some tendency toward off-centering, with signs of dynamic excited-state structural fluctuations observed in tellurium halides[88,90,91] and Cs_4MX_6.[37,92] The importance of such features in the optical performance will be discussed for the case of $5s^2$ metal halides based on Sb^{3+} and Sn^{2+}.

The $5s^2$ lone pair has an exceptionally rich chemistry because of the combination of stereoactivity and structural flexibility compared with neighboring metals. Following the inert pair effect, the oxidative stability of ns^2 cations increases moving down the periodic table, with $6s^2$ cations such as Pb^{2+} and Bi^{3+} having the most chemically inert lone pairs.[93,94] Lone pair electrons have strong stereochemical effects on the metal−ligand coordination environment; however, this lone pair expression is distinct from the chemical stability of the "inert" lone pair. The same larger $6s^2$ cations offer more space for the lone pair and reduced surface charge density on the cation than their lighter neighbors, increasing the polarizability and coordination number. These features permit structurally inert lone pairs such as the highly symmetric structures of PbI_2 and BiI_3, which have centered metal cations with no obvious lone pair expression.[69]

The 3D halide perovskites AMX_3 based on Ge^{2+}, Sn^{2+}, and Pb^{2+} are an instructive example to explore the differences between the $4s^2$, $5s^2$, and $6s^2$ lone pairs. The small size of the Ge^{2+} cation does not leave sufficient space for the lone pair electrons, and thus, $AGeX_3$ structures possess significant off-centering of the Ge atom toward a face of the would-be octahedron, leading to a trigonal-pyramidal coordination.[95] Sn^{2+}- and Pb^{2+}-based AMX_3 compounds exhibit perovskite-related structures with crystallographically inert lone pairs (with the exception of the highly distorted low-temperature phases of $MASnBr_3$),[96] but this belies a dynamic nature that leads to polar fluctuations at room temperature[5] and exceptional thermal expansion cofficients.[97] Stereochemical off-centering at high temperatures was first observed in $CsSnBr_3$, with the Sn atom exhibiting a trigonal shift toward the face of the octahedron with space group $R3m$,[98] exactly the same space group and off-centering found in the crystal structure of $AGeI_3$.[95] Subsequent studies have shown that this dynamic nature is more pronounced in the Sn^{2+} and Br^- analogues than in the respective Pb^{2+} or I^- compounds.[99]

This highlights that lone pair expression is also heavily influenced by the halogen size. For example, the binary halide $SnBr_2$ exhibits a different structure than $SnCl_2$, SnI_2, $PbCl_2$, and $PbBr_2$ because of the combination of stereochemical influence of its lone pair electrons with the appropriate size disparity between the metal and halogen, despite the fact that $SnCl_2$ exhibits the strongest repulsion of the lone pair.[100] Similarly, while BiI_3 adopts a layered structure with perfectly symmetric $[BiI_6]^{3-}$ octahedra, $BiCl_3$ exhibits trigonal distortions that lead to pyramidal coordination,[101] requiring additional crystal forces to return to the high-symmetry octahedra of Cs_3BiCl_6.[64] The smaller size of Sb causes all three binary halides SbX_3 (X = Cl, Br, I) to exhibit such off-centering,[101] but the templating influence of other cations can enforce high-symmetry crystallographic sites such as the $[SbCl_6]^{3-}$ octahedra in $Rb_7Sb_3Cl_{16}$[79] and $Cs_2NaSbCl_6$.[102] The case of $Cs_2NaSbCl_6$ is especially interesting, as the enforced octahedral symmetry on a normally expressed $SbCl_3$ lone pair leads to a large lattice constant of 10.7780 Å for $Cs_2NaSbCl_6$ while that of the isostructural $Cs_2NaInCl_6$ is 10.5313 Å,[102] despite the similar ionic radii of Sb^{3+} and In^{3+} (0.76 vs 0.80 Å).[103] This points to a dynamic distortion of the $[SbCl_6]^{3-}$ octahedron in which the stereochemistry of the lone pair is expressed dynamically while the cubic long-range symmetry is maintained.[29] However, this does not occur in the isostructural $Cs_2NaSbBr_6$, in which the ionic radius is consistent with the expected value,[29] highlighting the importance of metal−halogen overlap in determining the dynamics of the lone pair.

The contrast of lone pair stability and expression makes the $5s^2$ lone pair unique, as it lies on the cusp between the dynamically expressed lone pairs of $6s^2$ cations and the statically expressed lone pairs of the $4s^2$ cations. This interplay of dynamic and static off-centering is at its peak in the 0D $5s^2$ metal halides, permitting structural distortions that can yield efficient luminescence in materials where similar $4s^2$ or $6s^2$ structures have nonexistent or weak emission. For example, while Cs_4PbBr_6 does not emit at room temperature,[104,105] Cs_4SnBr_6 and $(C_4N_2H_{14}Br)_4SnBr_6$ have bright emission with PLQYs of 15%[37] and 95%,[19] respectively. This can be understood as a function of the enhanced hybridization between the metal ns^2 lone pair and the halide np orbitals, with recent work showing that the higher energy of the Sn 5s level leads to the trend $Cs_4SnBr_6 > Cs_4SnI_6 > Cs_4PbBr_6$ favoring efficient STE emission in the former while the latter only emits at low temperatures.[92] Similarly, in the disphenoidal metal bromides $(bmpip)_2MBr_4$, $(bmpip)_2SnBr_4$ has a PLQY of 75%, while that of $(bmpip)_2PbBr_4$ is only 24% and that of $(bmpip)_2GeBr_4$ is below 1%.[34] To better understand the broad, bright luminescence driven by the 0D $5s^2$ lone pair, we bridge together the various models that have been utilized to characterize this emission.

The contrast of lone pair stability and expression makes the $5s^2$ lone pair unique, as it lies on the cusp between the dynamically expressed lone pairs of $6s^2$ cations and the statically expressed lone pairs of the $4s^2$ cations.

https://dx.doi.org/10.1021/acsmaterialslett.0c00211
ACS Materials Lett. 2020, 2, 1218−1232

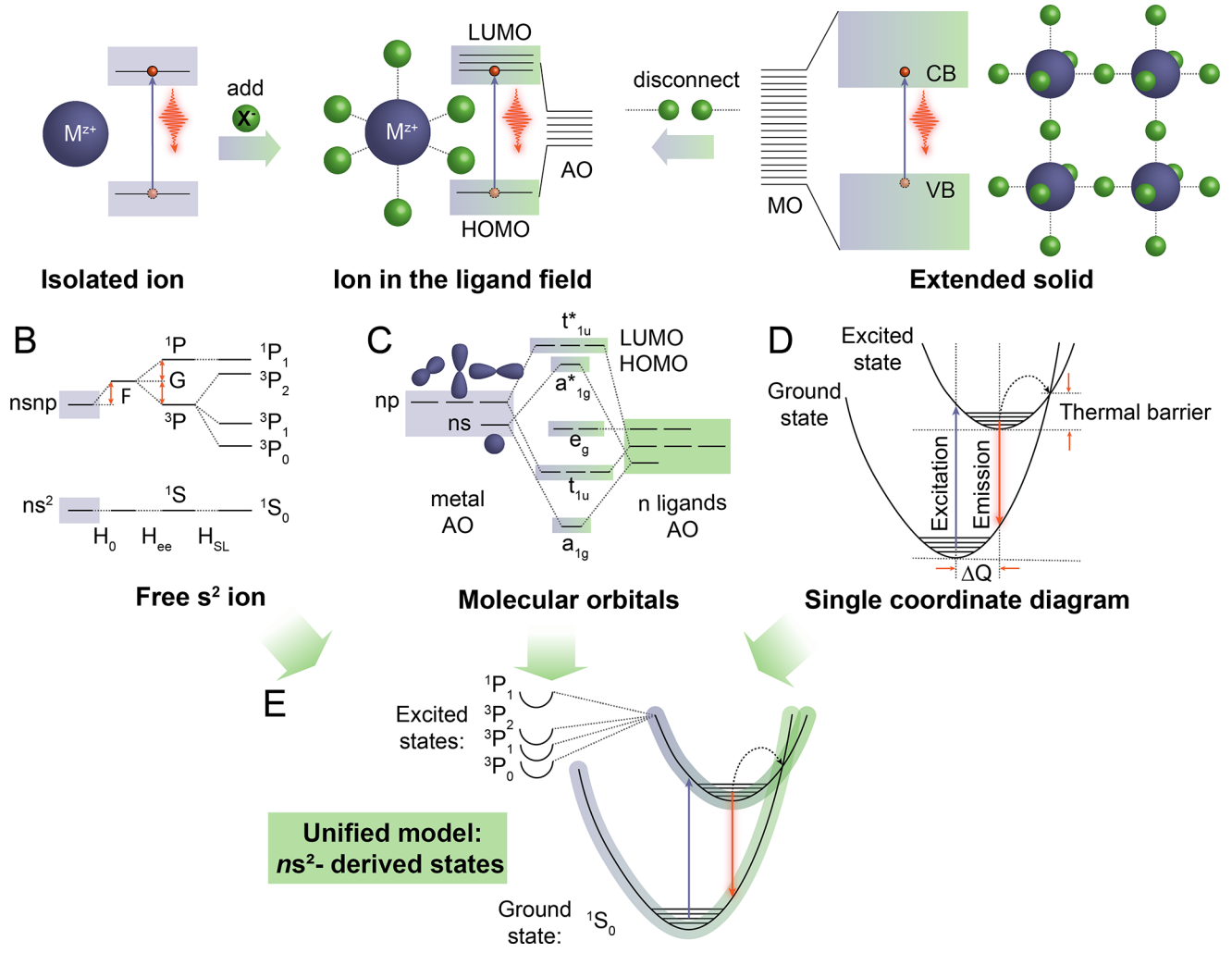

Figure 3. (A) Schematic representation of the relationship between the atomic orbital model, the molecular orbital model, and the semiconductor model of an extended solid. (B) Energy band diagram associated with the free ns^2 ion. (C) Energy band diagram of the metal–halide molecular orbitals. (D) Configurational coordinate diagram of the simplified STE model in 0D $5s^2$ metal halides. (E) Unified model with the configurational coordinate diagram, in which the ground and excited states are described using their atomic character as derived from the active ns^2 metal ion.

UNIFYING THEORY OF $5s^2$ EMISSION

Emission from the isolated center can manifest itself in many different forms, e.g., a dopant in a host matrix or pure material, as well as under different conditions, e.g., cryogenic or room temperature. Researchers from different fields of spectroscopy and materials science have contributed to isolated center emission studies. Because of this, different theoretical models are circulating in the literature. While these models share many features, the absence of a unified model (or the discussion of such a model) leads to contradicting and confusing terminology. Here we attempt to bring together the important theoretical concepts into a unified framework.

Two main models are presently utilized, arising from either (1) treating 0D centers as isolated ions dressed in the halide ligand field or (2) presenting these as the limiting case of complete electronic and structural isolation in the framework of an extended solid. Overall, both approaches lead to the same theoretical picture of the isolated MX_z centers, as illustrated in Figure 3A. Unification of the two models provides a framework that can explain and predict many properties of emissive 0D metal halides.

Unification of the two models provides a framework that can explain and predict many properties of emissive 0D metal halides.

The first theoretical description is derived from the simple two-electron Seitz model (Figure 3B). In this model, a free ion with the ns^2 configuration has the singlet electronic ground state, denoted with atomic term symbol $^1S_0$. The splitting of the $nsnp$ excited states into ^1P (singlet) and ^3P (triplet) states occurs as a result of the Coulomb (F) and exchange (G) interactions. Further, the ^3P states are split into non-degenerate states $^3P_2$, $^3P_1$, and $^3P_0$ by the spin–orbit coupling interaction. Additionally, the overall energy of all of the described states is non-uniformly altered by the ligand field (in this case by the coordinating halides). This interaction with the ligand field for ns^2 ions includes a large degree of hybridization between the atomic orbitals of the central metal and ligands, which is described by molecular orbital (MO) theory (Figure 3C). In this case, the ground and excited states are localized on both central ions and

https://dx.doi.org/10.1021/acsmaterialslett.0c00211
ACS Materials Lett. 2020, 2, 1218–1232

ligands. Atomic term symbols in this description are substituted with molecular term symbols (i.e., $^1S_0$ becomes a_{1g}). The relative energy of the latter depends directly on the molecular geometry (i.e., octahedral, square-pyramidal, disphenoidal) and has been summarized by Vogler and Nikol for different possible molecular geometries.[31] However, it remains very common in the literature to use atomic term symbols even for systems with a high degree of hybridization and denote the resulting molecular states as $^1P_1$-derived, $^3P_0$-derived, etc.[38,106,107] In this way, the model still serves its main purpose: to explain the transitions that occur between the states in terms of their allowed or forbidden nature, which can be experimentally reflected in the measured emission decay time (i.e., longer radiative lifetimes for partially forbidden transitions and shorter for allowed ones) or the intensity of the corresponding excitation band.[30,108]

For example, the dramatic reduction of the radiative lifetime of $Cs_2NaSbCl_6$ from 1.4 ms at 5 K to 0.15 μs at higher temperatures with no change in the emission intensity until ~200 K is derived entirely from changes in the character of the radiative excited state, from the forbidden $^3P_0 \rightarrow {}^1S_0$ transition at low temperatures to the $^3P_1 \rightarrow {}^1S_0$ transition by ~25 K.[29] On the other hand, the MO approach becomes useful for comparing optical properties for different geometries as well as correctly predicting the ground- and excited-state geometries. This is especially crucial for these 0D systems in which the halide bonds are not shared, and thus, the metal halide anion and its lone pair are free to distort in the excited state, and the excited-state geometry is dramatically different than the ground-state geometry.

Historically, the Seitz model was widely used to interpret the optical properties of ns^2 ion impurities in binary alkali metal halides[109] or in various other oxide and halide hosts.[29,30] The STE model for interpretation of the optical properties of 0D metal halides became widespread only recently because of the research focus on ns^2 metal halide semiconductors. While free excitons are dominant in the prototypical 3D AMX_3 semiconductors, the structural versatility of metal halides yields many compounds where STEs dominate.[50]

The typical theoretical description of phonon-assisted STE recombination involves a single configurational coordinate (SCC) diagram, in which the abscissa represents a change in molecular geometry upon excitation (Q) and the ordinate represents a change in energy (Figure 3D).[110] Ground and excited states in this model are described as parabolic potential energy functions, which are harmonic in the first approximation. It should be noted that in this SCC diagram, the free exciton excited state would be represented as a parabola centered at the ground state with higher energy;[57] however, free excitons have not been observed in 0D $5s^2$ metal halides, and hence, our model considers the localized self-trapped exciton as the only stable excited state. This is consistent with the description of Ueta et al. demonstrating that 1D or lower-dimensional systems have unstable free exciton states that localize upon any perturbation,[24] which means that the self-trapped exciton is the only relevant state in 0D $5s^2$ metal halides. This simplifies the STE model to an SCC diagram essentially identical to the generalized vibronic transitions described by the Franck–Condon principle. Here we maintain the use of the term "self-trapped exciton" to be consistent with the literature on higher-dimensional metal halides.

The minimum of each parabola represents the equilibrium geometry of the ground or excited state, while the horizontal difference between these geometries, ΔQ, is interpreted as the structural change that the metal halide center undergoes upon excitation. The difference between the excited- and ground-state geometries is reflected in the large Stokes shift of 0D $5s^2$ metal halide emission. Both absorption and emission transitions can occur from different vibronic states (denoted as flat lines in the parabola), thus yielding an amalgam of individual transitions with emission probabilities following a Poisson distribution. The convolution of these transitions results in a broadened emission peak, often with a tail toward lower energy.[59] The magnitude of the electron–phonon coupling is described by the Huang–Rhys parameter, which is larger for stronger coupling and defines the degree of broadening associated with STE emission.[59,110]

The STE model's configurational coordinate diagram is a simplified projection that represents a complex energy surface as a two-dimensional plot and therefore has limitations, especially in complex materials with multiple emissive centers. However, it has proven quite useful in characterizing STE emitters in recent years,[59,111,112] and in conjunction with the Toyozawa model,[24] important features such as the Huang–Rhys parameter and effective phonon energy can be derived. Importantly, this model also rationalizes a key property of STE emitters: temperature-dependent emission quenching.[24,108] The crossing of the ground- and excited-state parabolas provides a nonradiative relaxation pathway from the excited-state minimum to the crossing point purely through phonon excitation, known as hot nonradiative recombination.[24] The energy difference (height) between the intercept and the excited-state minimum defines the energy barrier (and thereby the temperature, as described further below) required to quench the radiative process (Figure 3D).

Thus, the Seitz model mainly focuses on the nature of the electronic states and, with the MO extension, on their degeneracy in the electric field of the ligand, while the SCC model describes phonon–exciton interactions. The successful interpretation of observed phenomena in the optical properties of 0D materials requires the aid of all three theoretical concepts. The unified model is depicted in Figure 3E. It is based on the SCC diagram, where the excited state can be split into several nondegenerate states, each reflecting the nature of the contributing atomic state. As we will show, the splitting and degeneracy of these states vary with the coordination geometry, but this model is flexible enough to describe the observed optical features.

PROPERTIES OF EMISSIVE $5s^2$ 0D MATERIALS

Among the various emissive $5s^2$ 0D materials that have been reported, the simplest case with which to study such structure–property relationships comes from Te^{4+}. The high charge of the metal center necessitates a greater number of halide ligands, restricting the known Te^{4+} halides to materials containing octahedrally coordinated Te^{4+} regardless of the nature of the countercation.[87,113] The most commonly adopted structure is that of the vacancy-ordered double perovskite A_2TeX_6 with regular octahedra.[87] The isostructural nature of these compounds has encouraged excellent fundamental studies; for example, the role of the halide in luminescence quenching has been studied in the series Cs_2TeX_6[114] and A_2TeX_6,[113] with chlorides showing the brightest emission at RT. The dynamic nature of these octahedra has also been extensively studied, with many reports on the dynamic Jahn–Teller effect-driven tetragonal distortions in the excited state.[86,88,90,113,115] The apparent simplicity of these materials, however, has not been manifested in numerous luminescent examples, as the

https://dx.doi.org/10.1021/acsmaterialslett.0c00211
ACS Materials Lett. 2020, 2, 1218–1232

Table 2. Summary of the Optical Properties of Highly Emissive 0D $5s^2$ Metal Halide Compounds

compound	coordination unit	$E_{exc/abs}$ (nm)	E_{em} (nm)	Stokes shift (eV)	FWHM (eV)	PLQY (%)	lifetime (μs)	ref
Cs_4SnBr_6	MX_6	340	540	1.28	0.51	15	0.54	37
HDM_3SnBr_8	MX_6	350	600	1.60	0.44	86	3.12	120
$(C_4N_2H_{14}Br)_4SnBr_6$	MX_6	355	570	1.32	0.40	95	2.2	19
$(PEA)_6SnBr_8[CCl_2H_2]_2$	MX_6	340	566	1.46	0.44	89.5	2.7	121
$(C_4N_2H_{14}I)_4SnI_6$	MX_6	410	620	1.02	0.38	75	1.1	19
$(bmpip)_2SnBr_4$	MX_4	350	658	1.66	0.37	75	4	34
$(C_6H_{22}N_4Cl_3)SnCl_3$	MX_3	280	638	2.48	0.42		7.6	71
$Bzmim_3SbCl_6$	MX_6	342	525	1.26		87.5	2.4	85
$Bzmim_2SbCl_5$	MX_5	375	600	1.24		22.3	2.6	85
$Bmim_2SbCl_5$	MX_5	370	583	1.22		86.3	4.26	18
$(C_9NH_{20})_2SbCl_5$	MX_5	380	590	1.16	0.43	98	4.2	19
TTA_2SbCl_5	MX_5	370	625	1.37	0.45	86	7.5	38
$TEBA_2SbCl_5$	MX_5	360	590	1.34	0.48	98	7.7	38
$(Ph_4P)_2SbCl_5$	MX_5	375	648	1.39	0.41	87	4.6	122
$(PPN)_2SbCl_5$	MX_5	410	635	1.07	0.44	98.1	4.1	119
$Rb_7Sb_3Cl_{16}$	MX_6, M_2X_{10}	365	560	1.16	0.53	3.8	0.2	79

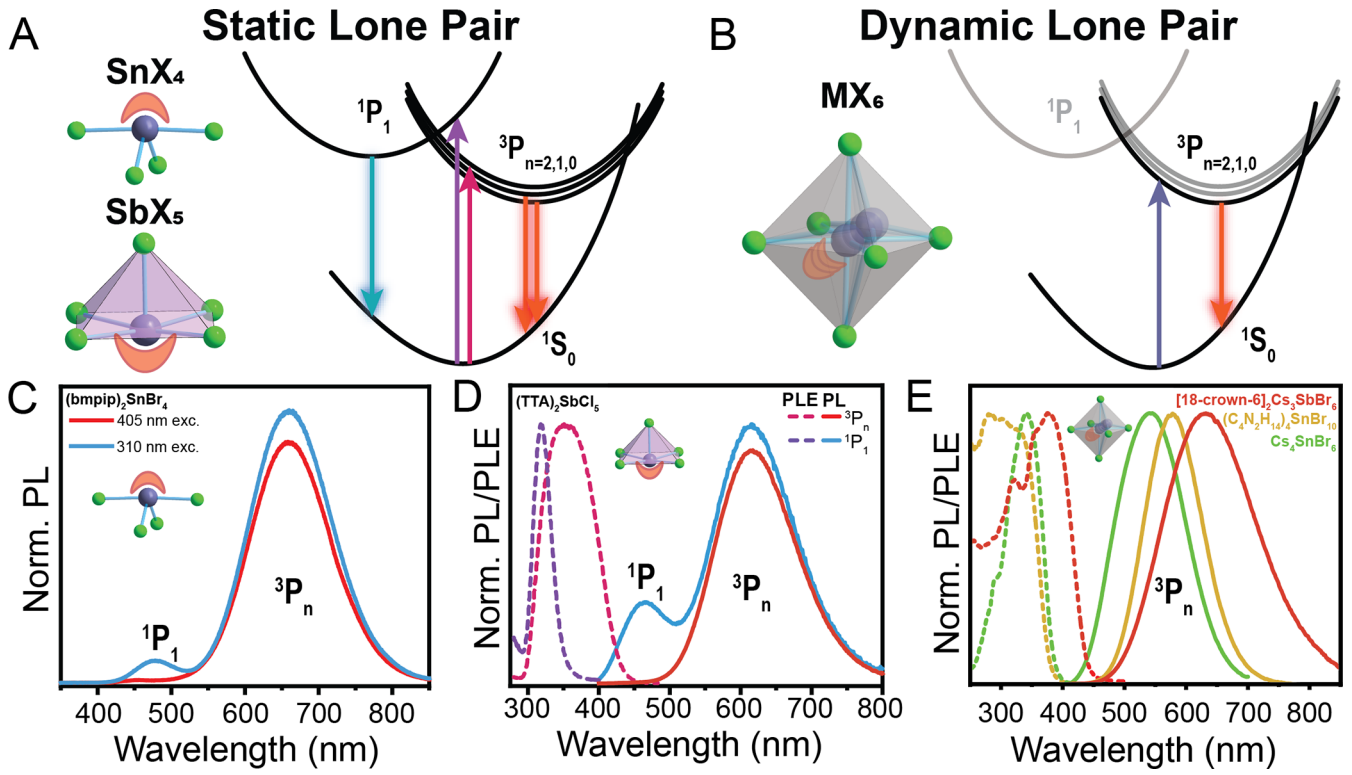

Figure 4. (A) 0D structures with statically expressed lone pairs (SnX_4, SbX_5) and the corresponding energy band diagram. (B) Dynamically distorted octahedral MX_6 and the corresponding band diagram. (C) Excitation-dependent PL of $(bmpip)_2SnBr_4$ showing singlet and triplet emission.[34] (D) PL and PL excitation (PLE) spectra of $(TTA)_2SbCl_5$ showing the separate excitation of the triplet and singlet states (reproduced using the previously reported synthesis[38] and characterized using an optical setup described elsewhere[34]). (E) PL and PLE spectra of Cs_4SnBr_6,[37] $(C_4N_2H_{14}Br)_4SnBr_6$,[19] and $[18\text{-crown-6}]_2Cs_3SbBr_6$.[118]

quenching temperatures are relatively low in these compounds,[86] and those that do emit at RT are plagued by low PLQYs. This appears to be due to an apparent concentration quenching effect[86] that is less pronounced in other $5s^2$ 0D metal halides, but the root cause deserves further investigation given the exceptional performance of Sn^{2+} and Sb^{3+} emissive materials and Te^{4+}'s distinct advantages of stability and its tendency to adopt a single coordination that encourages rational design.

At the other end of the spectrum, Sn^{2+} with its low charge exhibits the greatest structural diversity of 0D compounds, with examples of luminescent materials containing octahedra, disphenoids, and trigonal pyramids (Table 2 and Figure 4A). Additionally, a 0D structure containing square pyramids ($Rb_3SnCl_3I_2$) was also recently discovered; however, its potential for luminescence was left unexplored.[116] Though Sn^{2+} is a versatile ion for materials discovery, its tendency to oxidize to Sn^{4+} increases the synthetic difficulty of discovering new materials.[117] This may be one of the reasons why so far only seven room-temperature luminescent 0D structures have been

https://dx.doi.org/10.1021/acsmaterialslett.0c00211
ACS Materials Lett. 2020, 2, 1218−1232

reported. Of these, the most prominent examples consist primarily of disphenoids and octahedra (Figure 4).

Intermediate in 0D structural diversity is trivalent Sb^{3+}. Most of the luminescent examples in the literature are hybrid organic−inorganic materials with square-pyramidal $[SbCl_5]^{2-}$ units isolated by large organic cations (Figure 4A); the remainder are octahedral or polynuclear octahedral units obtained in cation/alkali halide-rich compositions, e.g., $(bzmim)_3SbCl_6$ and $Rb_7Sb_3Cl_{16}$ (Figure 4 and Table 2).

> Some empirical observations lead us to conclude that coordinatively unsaturated metal centers such as SnX_4 or MX_5 (M = Sn, Sb) can be obtained only through the use of organic and sufficiently bulky countercations or a combination of halides with very different sizes.

From a purely structural perspective, too few structures are known at this point to predict the structure-directing effect that a specific cation may have. However, some empirical observations lead us to conclude that coordinatively unsaturated metal centers such as SnX_4 or MX_5 (M = Sn, Sb) can be obtained only through the use of (a) organic and sufficiently bulky countercations (e.g., bmpip, PPh_4, bzmim, etc.; Table 2) or (b) a combination of halides with very different sizes (e.g., mixed Cl^-, I^-).[116] Smaller inorganic countercations can enable 0D structures in alkali halide-rich environments that sufficiently isolate the metal halide complex with high coordination numbers (e.g., Cs_4SnBr_6), but less alkali halide favors the formation of higher-dimensional frameworks (e.g., $CsSnBr_3$), as the small cations cannot fully isolate the 0D units (Table 1).

On the basis of these various Sn^{2+}- and Sb^{3+}-based materials, several examples can be compared to see how the geometry and the metal center affect the resulting optical properties. To examine these differences, the SCC diagrams for 0D Sn and Sb units can be redrawn on the basis of their geometry and the stereoactivity of the lone pair (Figure 4A,B). The "static" lone pair is expressed and found in coordinatively unsaturated geometries such as disphenoids (SnX_4) and square pyramids (SbX_5) (Figure 4A). In both cases, the reduced symmetry imposed by these motifs results in nondegenerate excited states, which may allow for additional transitions if the energy levels are sufficiently separated, although the separation may be quite small (Figure 4A).[31] This has been demonstrated by Morad et al., with the observation of both $^3P_1 \rightarrow {}^1S_0$ and $^1P_1 \rightarrow {}^1S_0$ transitions at RT in disphenoidal $(bmpip)_2SnBr_4$ (Figure 4C).[34] This also highlights the fact that the triplet STE state tends to be the lowest-energy excited state for such $5s^2$ metals. This same model extends to square-pyramidal Sb (i.e., MX_5 in Table 2), for which Wang et al. first observed two distinct emission bands from $(bmim)_2SbCl_5$,[18] and subsequently several other singlet-emitting hybrid antimony chlorides have been found.[19,119] One such compound is TTA_2SbCl_5, which further demonstrates the excitation-wavelength-dependent nature of the emission (Figure 4D).[38] High-energy excitation succeeds in populating the high-energy singlet $^1P_1$ state, resulting in emission directly from this state as well as emission from the thermodynamically favored lower-energy $^3P_1$ triplet state.

This situation is simplified in octahedrally coordinated systems (Figure 4B). The larger coordination number reduces the static expression of the lone pair and therefore off-centering and distortion, often leading to high-symmetry sites and similar bond lengths. The regularity (or near-regularity) of such sites obscures the optical properties present in the disphenoidal and square-pyramidal coordinations, as the dynamic distortions of these octahedra lead to stronger mixing of the excited states. This is best illustrated by comparing three $5s^2$ bromides: Cs_4SnBr_6, $(C_4N_2H_{14}Br)_4SnBr_6$, and $[18\text{-crown-6}]_2Cs_3SbBr_6$ (Figure 4E).[19,37,118] Although these three materials have

> Given the enormous diversity of structures offered by these $5s^2$ systems and their recent (re)discovery as optical materials, it is apparent that the community has only scratched the surface concerning their properties and how to utilize them.

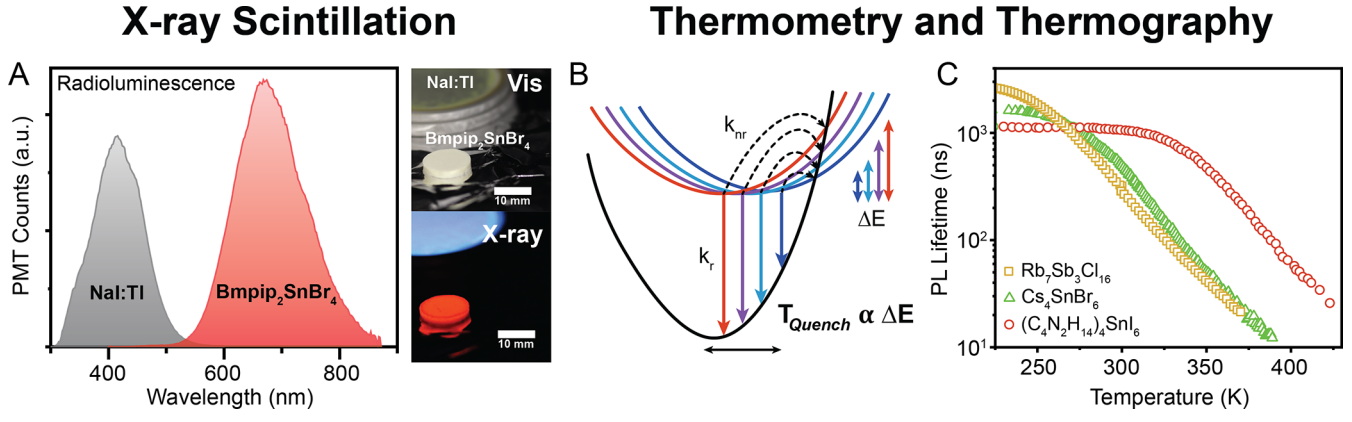

Figure 5. (A) Radioluminescence spectra of $(bmpip)_2SnBr_4$ and NaI:Tl under 50 kV Ag tube X-ray irradiation, with images of the NaI:Tl commercial scintillator and a $(bmpip)_2SnBr_4$ pellet under ambient light and X-ray irradiation. Adapted from ref 34. Copyright 2019 American Chemical Society. (B) Configurational coordinate diagram showing the change in energy barrier with different shifts of the excited state, with red and blue representing high and low ΔE (and thus quenching temperatures), respectively. (C) PL lifetime vs temperature for $Rb_7Sb_3Cl_{16}$,[79] Cs_4SnBr_6,[35] and $(C_4N_2H_{14}I)_4SnI_6$.[35]

https://dx.doi.org/10.1021/acsmaterialslett.0c00211
ACS Materials Lett. 2020, 2, 1218−1232

different metal centers and different degrees of distortion or lone pair expression, the PL spectra appear to be triplet ($^3P_{0,1,2}$)-dominated with one broad, featureless emission peak. This can be understood in terms of the higher degeneracy of the regular octahedral environment: while the trigonally distorted octahedron would have fully distinct singlet and triplet states, the regular octahedron does not fully separate these levels, and therefore, the singlet remains unobserved.[31] This also correlates with the reduced Stokes shift and emission line width in octahedral compounds relative to their more distorted counterparts; e.g., Vogler and Nikol compared the absorption and emission of disphenoidal $SbCl_4^-$ and octahedral $SbCl_6^{3-}$ in solution.[31]

Given the enormous diversity of structures offered by these $5s^2$ systems and their recent (re)discovery as optical materials, it is apparent that the community has only scratched the surface concerning their properties and how to utilize them. We highlight two rising applications that take advantage of the unique features of these 0D materials: X-ray scintillation and remote thermometry and thermography.

X-ray scintillation utilizes two features shared by these 0D $5s^2$ metal halide materials: (1) efficient relaxation processes for high-energy absorption to the STE triplet state and (2) highly Stokes-shifted emission such that the compounds are transparent to their emission. The first such study demonstrated that $(bmpip)_2SnBr_4$ could function as an excellent X-ray scintillator (Figure 5A).[34] A very recent work found that square-pyramidal $(PPN)_2SbCl_5$ also exhibits efficient X-ray scintillation,[119] and it is likely that many of these materials are radioluminescent. An open question is whether the long emission lifetimes (Table 2) are problematic for X-ray detection. Although these materials have low overall atomic numbers, they still perform comparably to commercially available NaI:Tl or CsI:Tl scintillators and seem to outperform organic scintillators. This class of materials deserves much more investigation in this context, and we hope to see collaborations between traditional scintillator groups and materials chemists to find effective scintillators among the $5s^2$ metal halides.

The second application, thermometry and thermography, is based on the steep temperature dependence of the PL lifetimes of these materials, as first demonstrated by our group for Cs_4SnBr_6, $(C_4N_2H_{14}I)_4SnI_6$, and $[C(NH_2)_3]_2SnBr_4$.[35] The PL lifetimes of these compounds vary by up to 2 orders of magnitude over a temperature range of 100 °C, giving rise to some of the highest specific sensitivities among known thermoluminophores. Temperature sensitivity is also observed in the PLQY of many materials, including these, but the dramatic changes in lifetime of 0D $5s^2$ metal halides impart a much stronger sensitivity than simply utilizing the emission intensity could provide.[35] This property is rationalized by the unified model presented earlier, which is simplified in Figure 5B to highlight the effect of shifting the excited-state parabola. The intersection of two parabolas (colored and black curves) represents a nonradiative pathway back to the ground state. As the Stokes shift increases and the material's PL red-shifts, the upper excited-state parabola shifts further from the ground-state parabola, lowering the energy barrier ΔE for the phonon-assisted "hot" nonradiative recombination.

Unlike conventional semiconductors, the PL lifetime in 0D metal halides is intrinsically robust, i.e., without noticeable effects of the structural defects and surfaces. This robust nature is a consequence of the strongly localized excited states of these 0D $5s^2$ metal halides, which lead to excited-state energy bands with high Stokes shifts and momentum offsets that inhibit nonradiative recombination from defect states and favor hot recombination. The only other known source of nonradiative quenching comes from parasitic impurity phases such as $CsSnBr_3$, which absorbs in the emissive region of Cs_4SnBr_6,[37] but such quenching is only known to affect the PLQY.

Thus, hot nonradiative recombination dominates in 0D $5s^2$ metal halides, dictated by the energy barrier ΔE that governs the quenching temperature of the luminescence, T_{quench}. ΔE, along with the average or effective phonon energy, E_{ph}, directly influences the emission lifetime and PLQY through the temperature-dependent competition between the radiative and nonradiative relaxation rates (k_r vs k_{nr}, respectively). The onset of quenching, with corresponding changes in lifetime, defines the temperature-sensitive regime. For example, in Figure 5C this regime is found at the higher temperatures, where k_r and k_{nr} compete effectively against one another and k_r remains non-negligible. In contrast, the flat region at low temperatures (<325 K for $(C_4N_2H_{14}I)_4SnI_6$; <250 K for Cs_4SnBr_6 and $Rb_7Sb_3Cl_{16}$) involves a purely radiative process, where k_{nr} is negligible, and the PL lifetime remains rather unaltered and the PLQY is saturated. This trend appears to be general not only for 0D Sn materials but also for 0D Sb materials (Figure 5C).[79] This robust thermal sensitivity, which can be tuned by structural engineering, and the wide temperature and lifetime ranges that it covers make $5s^2$ metal halides a compelling class of novel thermoluminophores.

Cryogenic temperatures can present exceptions to this behavior that may also prove suitable for thermometric applications, as below 77 K in $Rb_7Sb_3Cl_{16}$ a second temperature-sensitive regime can be observed without any change in the PLQY.[79] This purely radiative yet thermally sensitive regime is likely driven by changes in the character of the excited-state levels, as described above for $Cs_2NaSbCl_6$.[29,108] The unchanging intensity with concurrent temperature sensitivity ensures that the signal from the thermometric probe will remain strong throughout the entire sensitivity regime. This unique behavior may enable high thermometric sensitivities at extremely low temperatures (below 10−15 K), where accurate temperature values can be difficult to obtain through other means without altering the temperature of the system and hence a simple optical probe may be quite valuable.

POLYNUCLEAR 0D $5s^2$ COMPOUNDS

Beyond these isolated 0D units, a plethora of polynuclear 0D cluster compounds based on $5s^2$ metal cations exist.[43,78,87,123] Their optical potential remains to be thoroughly explored. RT PL has been reported for $[Sb_2I_9]^{3-}$ dimers in $Cs_3Sb_2I_9$, but with rather weak emission intensity.[59] This may be due to the asymmetry in these polynuclear systems, which provides stable lone pair off-centering in coupled units that may enhance nonradiative recombination (Figure 6). However, the discovery of $Rb_7Sb_3Cl_{16}$ and its emissive distorted $[Sb_2Cl_{10}]^{4-}$ dimer with a PLQY of 3.8% demonstrates that there are more optically active centers to be discovered.[79] Recent reports on a bright $[Pb_3Cl_{11}]^{5-}$ cluster with near-unity PLQY provide further encouragement,[124] and we expect emissive clusters to be a rich avenue of exploration moving forward.

OTHER EMISSIVE METAL CENTERS

We also wish to highlight a recent series of metal halides based on ns^0 (d^{10}) cations that have exhibited remarkably efficient and

https://dx.doi.org/10.1021/acsmaterialslett.0c00211
ACS Materials Lett. 2020, 2, 1218−1232

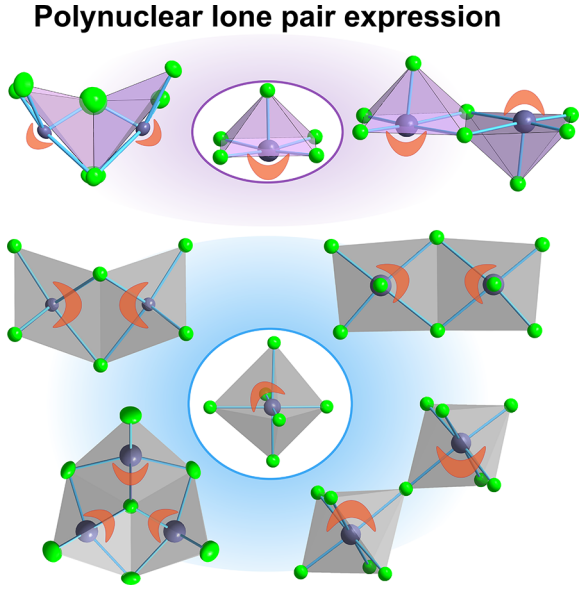

Figure 6. Atomic environments of polynuclear 0D $5s^2$ metal halides derived from square pyramids and octahedra, with the lone pairs visualized in orange.

broadband luminescence similar to that observed in the $5s^2$ metal halides. Examples of nd^{10} emitters have been known for many years among the Cu^+ and Ag^+ halides,[125−127] but this field has been reinvigorated with a flurry of investigations in the last 5 years showcasing the utility of these materials in scintillators and light-emitting diodes (LEDs).[128−131] This group has been further bolstered by several new broadband-emissive compounds based on isoelectronic Zn^{2+} and Cd^{2+}.[132−135] Mixing of $nd^{10}ns^2$ systems has also led in some cases to enhanced emission,[136] and we expect that there is much more synergy to be found among such mixed-metal systems. In particular, combining the efficient excitation of low-band-gap ns^2-based materials with highly emissive nd^{10} centers could make for attractive white-light phosphors.

In the case of In^{3+}, the reported emission characteristics are extraordinarily similar to those of Sb^{3+}-doped indium halide materials.[39,137−139] A new report found that undoped and Sb^{3+}-doped $Cs_2InCl_5{\cdot}H_2O$ had essentially identical features and temperature-dependent intensities,[39] while recent work in our group showed that pure $Cs_2NaInCl_6$ and $Cs_2InCl_5{\cdot}H_2O$ do not emit.[140] In our view, trace Sb^{3+} dopants in the precursors may be responsible for these emissions, similar to the miniscule levels of Sn impurities that were found by Mitzi et al. to generate STE emission in PEA_2PbBr_4.[141] Careful experimental work would be required to demonstrate this, perhaps utilizing InX monohalides as indium precursors that would be chemically less likely to contain trace Sb^{3+} impurities. A very recent report further validates this view by demonstrating that pure $Cs_2InCl_5{\cdot}H_2O$ does not luminesce without Sb^{3+} doping.[107]

SUMMARY AND OUTLOOK

The future is bright for emissive lone pair materials, and the structural versatility of $5s^2$ metal halides yields a wide compositional space for the design of emitters with unique properties. Low-dimensional emissive $5s^2$ metal halides offer several advantages: quantum efficiencies near unity; earth-abundant, nontoxic metal cations; intrinsic emission that does not require doping, electronic passivation or particle size control to achieve high performance; and large Stokes shifts that minimize self-absorption. Applications of such compounds include X-ray scintillation, phosphors for white-light emission, and high-resolution thermography, and we expect great strides in each of these fields in the coming years. That being said, challenges persist that will need to be overcome to enable the development of successful devices that fulfill the promise of these applications.

Many open questions deserve further exploration to understand the structure−property relationships and unveil the practical potential of these compounds. At present, it is difficult to predict the coordination environment generated by different organic cations, and finding design principles will require many more examples to tease out the effects of cation size, polarity, bonding characteristics, etc. Even in the absence of such design principles, several important trends can be observed on the basis of the available literature. For example, nearly all examples of highly emissive compounds in Table 2 can be grouped into two kinds, namely, Sn(II) bromides and Sb(III) chlorides, indicating that the orbital overlap and/or phonon energies in these combinations are particularly suited for highly efficient emission. In the Cs_2TeX_6 system, the RT emission intensity increases for lighter halides, similar to Sb(III) halides but contrary to Sn(II) bromides. Further studies, such as the computational comparison of Cs_4SnBr_6, Cs_4SnI_6, and Cs_4PbBr_6 that identified the importance of the Sn $5s^2$−Br 4p overlap,[92] are needed to determine whether the energy levels of Sn(II) and Br are ideal for efficient emission or whether the lower stability of Sn(II) chlorides is the key to the observed differences. The structural and photophysical aspects of the excited state are rather poorly understood. While we have elaborated on some intriguing trends in the structure−property relationships of these compounds and the connection to the $5s^2$ lone pair, a true picture of the dynamics of these systems is currently lacking. Besides commonplace transient absorption spectroscopy, excited states of these materials can be probed by ultrafast measurements that combine optical excitation and structure probing (ultrafast electron or X-ray scattering).[50,57,99,142−144]

We also observe that the hybrid organic−inorganic materials routinely exhibit higher PLQYs than their fully inorganic counterparts, which may indicate more effective 0D isolation in the former materials with large and soft organic cations (Table 2). This likely derives from the lower-energy phonons and their enhanced coupling in inorganic materials, whereas the high-energy phonons of the organics improve the structural isolation of the lone-pair-driven vibrational modes in these 0D materials and push the temperature region for thermal quenching to higher temperatures (Figure 5C). However, the inorganic compositions benefit from enhanced stability and higher melting points, as manifested in the ability to prepare nanocrystals (NCs) of Cs_4SnBr_6,[145,146] which has not yet been demonstrated for any hybrid organic−inorganic 0D compositions.

The properties that allow them to excel as thermosensitive phosphors may hinder the utility of metal halides as solid-state lighting phosphors. During LED operation, the excitation source typically heats the phosphor, with local surface temperatures potentially exceeding 70 °C.[147,148] While hybrid organic−inorganic metal halides generally exhibit higher PLQYs at ambient and elevated temperatures, their chemical stability becomes a limiting factor. Furthermore, the majority of these materials exhibit excitation peaks below 400 nm, which are unsuitable for use even with purple LEDs (405 nm) and require them to be paired with UV LEDs (for which an inexpensive and

https://dx.doi.org/10.1021/acsmaterialslett.0c00211
ACS Materials Lett. 2020, 2, 1218−1232

efficient UV light source is unavailable at present) for use as downconversion phosphors in white-light LEDs.[149] The combination of these two limitations necessitates further structural exploration of $5s^2$-based materials suitable for white-light LEDs.

With regard to application in scintillators, a pertinent challenge is their intrinsically slow radiative recombination, in the low microsecond range (Table 2). Time-resolved radioluminescence studies are needed to determine the decay time under X-ray excitation and the possibility of afterglow. These compounds may therefore not be suitable for applications that require photon counting and/or spectroscopic X-ray energy resolution capabilities, such as positron emission tomography and nuclear security. However, static X-ray imaging such as used in dental and physician practices would benefit from the low-cost nature of these materials and the high reported sensitivity,[119] which enables a low dose rate to the patient.

So far, we have found that emission characteristics and durability of known $5s^2$ metal halides neatly match the theoretical and practical requirements of thermometric applications. The intrinsic nature of the STE emission makes the emission characteristics rather insensitive to the particle size, surface, and common structural defects and hence the synthesis method. The temperature range of high sensitivity is exceptional and broadly tunable by chemical design, while the respective PL lifetimes lie in convenient ranges for various detection schemes (ns to μs). Future work should also focus on the design of nanoscopic thermoluminescent probes. This requires the synthesis of size-tunable and environmentally stable nanoparticles of 0D metal halides. For high-resolution thermal imaging of biological systems, these NCs must be water-compatible and water-dispersible.

The intrinsic nature of the STE emission makes the emission characteristics rather insensitive to the particle size, surface, and common structural defects and hence the synthesis method.

AUTHOR INFORMATION

Corresponding Author

Maksym V. Kovalenko − *Laboratory of Inorganic Chemistry, Department of Chemistry and Applied Biosciences, ETH Zürich, CH-8093 Zürich, Switzerland; Laboratory for Thin Films and Photovoltaics, Empa—Swiss Federal Laboratories for Materials Science and Technology, CH-8600 Dübendorf, Switzerland;* orcid.org/0000-0002-6396-8938; Email: mvkovalenko@ethz.ch

Authors

Kyle M. McCall − *Laboratory of Inorganic Chemistry, Department of Chemistry and Applied Biosciences, ETH Zürich, CH-8093 Zürich, Switzerland; Laboratory for Thin Films and Photovoltaics, Empa—Swiss Federal Laboratories for Materials Science and Technology, CH-8600 Dübendorf, Switzerland;* orcid.org/0000-0001-8628-3811

Viktoriia Morad − *Laboratory of Inorganic Chemistry, Department of Chemistry and Applied Biosciences, ETH Zürich, CH-8093 Zürich, Switzerland; Laboratory for Thin Films and Photovoltaics, Empa—Swiss Federal Laboratories for Materials Science and Technology, CH-8600 Dübendorf, Switzerland*

Bogdan M. Benin − *Laboratory of Inorganic Chemistry, Department of Chemistry and Applied Biosciences, ETH Zürich, CH-8093 Zürich, Switzerland; Laboratory for Thin Films and Photovoltaics, Empa—Swiss Federal Laboratories for Materials Science and Technology, CH-8600 Dübendorf, Switzerland*

Complete contact information is available at: https://pubs.acs.org/10.1021/acsmaterialslett.0c00211

Notes

The authors declare no competing financial interest.

Biographies

Kyle M. McCall received his Ph.D. in Applied Physics from Northwestern University in 2019 under the joint supervision of Professors Mercouri Kanatzidis and Bruce Wessels. He is now working as a postdoctoral researcher under Professor Maksym V. Kovalenko in the Functional Inorganic Materials laboratory at ETH Zürich. His research interests focus on halide materials for radiation detection and light emission.

Viktoriia Morad received her M.S. in Chemistry from ETH Zürich in 2018 and since then has been pursuing a Ph.D. under the supervision of Prof. Maksym V. Kovalenko at ETH Zürich. Her research is focused on synthesis and applications of metal halides for light emission.

Bogdan M. Benin received his M.S. in Chemistry from Kent State University in 2016 and is now pursuing his Ph.D. under the supervision of Prof. Dr. Maksym V. Kovalenko at ETH Zürich. His research currently focuses on the discovery and application of luminescent zero-dimensional lead-free metal halides.

Maksym V. Kovalenko received his Ph.D. from Johannes Kepler University Linz in 2007 and was a postdoctoral researcher at the University of Chicago in 2008−2011. Since 2011 he has led the Functional Inorganic Materials group at ETH Zürich and Empa. He has been a full professor since 2020. The research activities of his group focus on discovery and engineering of novel inorganic materials and their applications for light emission and detection as well as in rechargeable batteries.

ACKNOWLEDGMENTS

This work was financially supported by ETH Zürich through the ETH+ Project SynMatLab and by the European Union through the Horizon 2020 Research and Innovation Programme (Grant Agreement 819740, Project SCALE-HALO). The authors thank Rebecca McClain for constructive input in figure design.

REFERENCES

(1) Stoumpos, C. C.; Kanatzidis, M. G. The Renaissance of Halide Perovskites and Their Evolution as Emerging Semiconductors. *Acc. Chem. Res.* **2015**, *48*, 2791−2802.

(2) Saparov, B.; Mitzi, D. B. Organic−Inorganic Perovskites: Structural Versatility for Functional Materials Design. *Chem. Rev.* **2016**, *116*, 4558−4596.

(3) Miyata, K.; Atallah, T. L.; Zhu, X. Y. Lead halide perovskites: Crystal−liquid duality, phonon glass electron crystals, and large polaron formation. *Sci. Adv.* **2017**, *3*, e1701469.

(4) Stoumpos, C. C.; Malliakas, C. D.; Kanatzidis, M. G. Semiconducting Tin and Lead Iodide Perovskites with Organic Cations: Phase Transitions, High Mobilities, and Near-Infrared Photoluminescent Properties. *Inorg. Chem.* **2013**, *52*, 9019−9038.

(5) Yaffe, O.; Guo, Y.; Tan, L. Z.; Egger, D. A.; Hull, T.; Stoumpos, C. C.; Zheng, F.; Heinz, T. F.; Kronik, L.; Kanatzidis, M. G.; Owen, J. S.; Rappe, A. M.; Pimenta, M. A.; Brus, L. E. Local Polar Fluctuations in Lead Halide Perovskite Crystals. *Phys. Rev. Lett.* **2017**, *118*, 136001.

(6) Wright, A. D.; Verdi, C.; Milot, R. L.; Eperon, G. E.; Perez-Osorio, M. A.; Snaith, H. J.; Giustino, F.; Johnston, M. B.; Herz, L. M. Electron−phonon coupling in hybrid lead halide perovskites. *Nat. Commun.* **2016**, *7*, 11755.
(7) Miyata, K.; Meggiolaro, D.; Trinh, M. T.; Joshi, P. P.; Mosconi, E.; Jones, S. C.; De Angelis, F.; Zhu, X. Y. Large polarons in lead halide perovskites. *Sci. Adv.* **2017**, *3*, e1701217.
(8) Stranks, S. D.; Eperon, G. E.; Grancini, G.; Menelaou, C.; Alcocer, M. J. P.; Leijtens, T.; Herz, L. M.; Petrozza, A.; Snaith, H. J. Electron−Hole Diffusion Lengths Exceeding 1 Micrometer in an Organometal Trihalide Perovskite Absorber. *Science* **2013**, *342*, 341.
(9) He, Y.; Matei, L.; Jung, H. J.; McCall, K. M.; Chen, M.; Stoumpos, C. C.; Liu, Z.; Peters, J. A.; Chung, D. Y.; Wessels, B. W.; Wasielewski, M. R.; Dravid, V. P.; Burger, A.; Kanatzidis, M. G. High spectral resolution of gamma-rays at room temperature by perovskite $CsPbBr_3$ single crystals. *Nat. Commun.* **2018**, *9*, 1609.
(10) Kovalenko, M. V.; Protesescu, L.; Bodnarchuk, M. I. Properties and potential optoelectronic applications of lead halide perovskite nanocrystals. *Science* **2017**, *358*, 745.
(11) Kang, J.; Wang, L.-W. High Defect Tolerance in Lead Halide Perovskite $CsPbBr_3$. *J. Phys. Chem. Lett.* **2017**, *8*, 489−493.
(12) Xiao, Z.; Song, Z.; Yan, Y. From Lead Halide Perovskites to Lead-Free Metal Halide Perovskites and Perovskite Derivatives. *Adv. Mater.* **2019**, *31*, 1803792.
(13) Chung, I.; Song, J.-H.; Im, J.; Androulakis, J.; Malliakas, C. D.; Li, H.; Freeman, A. J.; Kenney, J. T.; Kanatzidis, M. G. $CsSnI_3$: Semiconductor or Metal? High Electrical Conductivity and Strong Near-Infrared Photoluminescence from a Single Material. High Hole Mobility and Phase-Transitions. *J. Am. Chem. Soc.* **2012**, *134*, 8579−8587.
(14) Saparov, B.; Hong, F.; Sun, J.-P.; Duan, H.-S.; Meng, W.; Cameron, S.; Hill, I. G.; Yan, Y.; Mitzi, D. B. Thin-Film Preparation and Characterization of $Cs_3Sb_2I_9$: A Lead-Free Layered Perovskite Semiconductor. *Chem. Mater.* **2015**, *27*, 5622−5632.
(15) Lehner, A. J.; Fabini, D. H.; Evans, H. A.; Hébert, C.-A.; Smock, S. R.; Hu, J.; Wang, H.; Zwanziger, J. W.; Chabinyc, M. L.; Seshadri, R. Crystal and Electronic Structures of Complex Bismuth Iodides $A_3Bi_2I_9$ (A = K, Rb, Cs) Related to Perovskite: Aiding the Rational Design of Photovoltaics. *Chem. Mater.* **2015**, *27*, 7137−7148.
(16) Stoumpos, C. C.; Cao, D. H.; Clark, D. J.; Young, J.; Rondinelli, J. M.; Jang, J. I.; Hupp, J. T.; Kanatzidis, M. G. Ruddlesden−Popper Hybrid Lead Iodide Perovskite 2D Homologous Semiconductors. *Chem. Mater.* **2016**, *28*, 2852−2867.
(17) McClure, E. T.; Ball, M. R.; Windl, W.; Woodward, P. M. Cs_2AgBiX_6 (X = Br, Cl): New Visible Light Absorbing, Lead-Free Halide Perovskite Semiconductors. *Chem. Mater.* **2016**, *28*, 1348−1354.
(18) Wang, Z.-P.; Wang, J.-Y.; Li, J.-R.; Feng, M.-L.; Zou, G.-D.; Huang, X.-Y. $[Bmim]_2SbCl_5$: a main group metal-containing ionic liquid exhibiting tunable photoluminescence and white-light emission. *Chem. Commun.* **2015**, *51*, 3094−3097.
(19) Zhou, C.; Lin, H.; Tian, Y.; Yuan, Z.; Clark, R.; Chen, B.; van de Burgt, L. J.; Wang, J. C.; Zhou, Y.; Hanson, K.; Meisner, Q. J.; Neu, J.; Besara, T.; Siegrist, T.; Lambers, E.; Djurovich, P.; Ma, B. Luminescent zero-dimensional organic metal halide hybrids with near-unity quantum efficiency. *Chem. Sci.* **2018**, *9*, 586−593.
(20) Milot, R. L.; Sutton, R. J.; Eperon, G. E.; Haghighirad, A. A.; Martinez Hardigree, J.; Miranda, L.; Snaith, H. J.; Johnston, M. B.; Herz, L. M. Charge-Carrier Dynamics in 2D Hybrid Metal−Halide Perovskites. *Nano Lett.* **2016**, *16*, 7001−7007.
(21) Hong, X.; Ishihara, T.; Nurmikko, A. V. Dielectric confinement effect on excitons in PbI4-based layered semiconductors. *Phys. Rev. B: Condens. Matter Mater. Phys.* **1992**, *45*, 6961−6964.
(22) Xiao, Z.; Meng, W.; Wang, J.; Mitzi, D. B.; Yan, Y. Searching for promising new perovskite-based photovoltaic absorbers: the importance of electronic dimensionality. *Mater. Horiz.* **2017**, *4*, 206−216.
(23) Meng, W.; Wang, X.; Xiao, Z.; Wang, J.; Mitzi, D. B.; Yan, Y. Parity-Forbidden Transitions and Their Impact on the Optical Absorption Properties of Lead-Free Metal Halide Perovskites and Double Perovskites. *J. Phys. Chem. Lett.* **2017**, *8*, 2999−3007.
(24) Ueta, M.; Kanzaki, H.; Kobayashi, K.; Toyozawa, Y.; Hanamura, E. Theory of Excitons in Phonon Fields. In *Excitonic Processes in Solids*; Springer: Berlin, 1986; pp 203−284.
(25) Williams, R. T.; Song, K. S. The self-trapped exciton. *J. Phys. Chem. Solids* **1990**, *51*, 679−716.
(26) Smith, M. D.; Jaffe, A.; Dohner, E. R.; Lindenberg, A. M.; Karunadasa, H. I. Structural origins of broadband emission from layered Pb−Br hybrid perovskites. *Chem. Sci.* **2017**, *8*, 4497−4504.
(27) Knox, R. S. Introduction to Exciton Physics. In *Collective Excitations in Solids*; Di Bartolo, B., Ed.; Springer: Boston, 1983; pp 183−245.
(28) Timmermans, C. W. M.; Blasse, G. The Luminescence of $K_4Bi_2Br_{10}{\cdot}4H_2O$ and Rb_3BiBr_6 Single Crystals. *Phys. Status Solidi B* **1983**, *118*, 353−361.
(29) Oomen, E. W. J. L.; Smit, W. M. A.; Blasse, G. The luminescence of $Cs_2NaSbCl_6$ and $Cs_2NaSbBr_6$: a transition from a localized to a delocalized excited state. *Chem. Phys. Lett.* **1987**, *138*, 23−28.
(30) Blasse, G. Interaction Between Optical Centers and their Surroundings: An Inorganic Chemist's Approach. *Adv. Inorg. Chem.* **1990**, *35*, 319−402.
(31) Vogler, A.; Nikol, H. The Structures of s^2 Metal Complexes in the Ground and sp Excited States. *Comments Inorg. Chem.* **1993**, *14*, 245−261.
(32) Zhou, G.; Su, B.; Huang, J.; Zhang, Q.; Xia, Z. Broad-band emission in metal halide perovskites: Mechanism, materials, and applications. *Mater. Sci. Eng., R* **2020**, *141*, 100548.
(33) Shimizu, M.; Koshimizu, M.; Fujimoto, Y.; Yanagida, T.; Ono, S.; Asai, K. Luminescence and scintillation properties of Cs_3BiCl_6 crystals. *Opt. Mater.* **2016**, *61*, 115−118.
(34) Morad, V.; Shynkarenko, Y.; Yakunin, S.; Brumberg, A.; Schaller, R. D.; Kovalenko, M. V. Disphenoidal Zero-Dimensional Lead, Tin, and Germanium Halides: Highly Emissive Singlet and Triplet Self-Trapped Excitons and X-ray Scintillation. *J. Am. Chem. Soc.* **2019**, *141*, 9764−9768.
(35) Yakunin, S.; Benin, B. M.; Shynkarenko, Y.; Nazarenko, O.; Bodnarchuk, M. I.; Dirin, D. N.; Hofer, C.; Cattaneo, S.; Kovalenko, M. V. High-resolution remote thermometry and thermography using luminescent low-dimensional tin-halide perovskites. *Nat. Mater.* **2019**, *18*, 846−852.
(36) Zhou, C.; Lin, H.; Shi, H.; Tian, Y.; Pak, C.; Shatruk, M.; Zhou, Y.; Djurovich, P.; Du, M.; Ma, B. A Zero-Dimensional Organic Seesaw-Shaped Tin Bromide with Highly Efficient Strongly Stokes-Shifted Deep-Red Emission. *Angew. Chem., Int. Ed.* **2018**, *57*, 1021−1024.
(37) Benin, B. M.; Dirin, D. N.; Morad, V.; Wörle, M.; Yakunin, S.; Rainò, G.; Nazarenko, O.; Fischer, M.; Infante, I.; Kovalenko, M. V. Highly Emissive Self-Trapped Excitons in Fully Inorganic Zero-Dimensional Tin Halides. *Angew. Chem., Int. Ed.* **2018**, *57*, 11329−11333.
(38) Li, Z.; Li, Y.; Liang, P.; Zhou, T.; Wang, L.; Xie, R.-J. Dual-Band Luminescent Lead-Free Antimony Chloride Halides with Near-Unity Photoluminescence Quantum Efficiency. *Chem. Mater.* **2019**, *31*, 9363−9371.
(39) Liu, X.; Xu, X.; Li, B.; Liang, Y.; Li, Q.; Jiang, H.; Xu, D. Antimony-Doping Induced Highly Efficient Warm-White Emission in Indium-Based Zero-Dimensional Perovskites. *CCS Chem.* **2020**, *2*, 216−224.
(40) Spanopoulos, I.; Hadar, I.; Ke, W.; Guo, P.; Sidhik, S.; Kepenekian, M.; Even, J.; Mohite, A. D.; Schaller, R. D.; Kanatzidis, M. G. Water Stable 1D Hybrid Tin(II) Iodide Emits Broad Light with 36% Photoluminescence Quantum Efficiency. *J. Am. Chem. Soc.* **2020**, *142*, 9028−9038.
(41) Stoumpos, C. C.; Mao, L.; Malliakas, C. D.; Kanatzidis, M. G. Structure−Band Gap Relationships in Hexagonal Polytypes and Low-Dimensional Structures of Hybrid Tin Iodide Perovskites. *Inorg. Chem.* **2017**, *56*, 56−73.
(42) Kamminga, M. E.; Fang, H.-H.; Filip, M. R.; Giustino, F.; Baas, J.; Blake, G. R.; Loi, M. A.; Palstra, T. T. M. Confinement Effects in Low-

Dimensional Lead Iodide Perovskite Hybrids. *Chem. Mater.* **2016**, *28*, 4554−4562.
(43) Fisher, G. A.; Norman, N. C. The Structures of the Group 15 Element(III) Halides and Halogenoanions. *Adv. Inorg. Chem.* **1994**, *41*, 233−271.
(44) Wu, L.-M.; Wu, X.-T.; Chen, L. Structural overview and structure−property relationships of iodoplumbate and iodobismuthate. *Coord. Chem. Rev.* **2009**, *253*, 2787−2804.
(45) Sobczyk, L.; Jakubas, R.; Zaleski, J. Self-assembly of Sb(III) and Bi(III) halo-coordinated octahedra in salts of organic cations. Structure, properties and phase transitions. *Pol. J. Chem.* **1997**, *71*, 265−300.
(46) Glazer, A. The classification of tilted octahedra in perovskites. *Acta Crystallogr., Sect. B: Struct. Crystallogr. Cryst. Chem.* **1972**, *28*, 3384−3392.
(47) Pazos-Outón, L. M.; Szumilo, M.; Lamboll, R.; Richter, J. M.; Crespo-Quesada, M.; Abdi-Jalebi, M.; Beeson, H. J.; Vrućinić, M.; Alsari, M.; Snaith, H. J.; Ehrler, B.; Friend, R. H.; Deschler, F. Photon recycling in lead iodide perovskite solar cells. *Science* **2016**, *351*, 1430.
(48) Richter, J. M.; Abdi-Jalebi, M.; Sadhanala, A.; Tabachnyk, M.; Rivett, J. P. H.; Pazos-Outón, L. M.; Gödel, K. C.; Price, M.; Deschler, F.; Friend, R. H. Enhancing photoluminescence yields in lead halide perovskites by photon recycling and light out-coupling. *Nat. Commun.* **2016**, *7*, 13941.
(49) Zhou, C.; Lin, H.; He, Q.; Xu, L.; Worku, M.; Chaaban, M.; Lee, S.; Shi, X.; Du, M.-H.; Ma, B. Low dimensional metal halide perovskites and hybrids. *Mater. Sci. Eng., R* **2019**, *137*, 38−65.
(50) Smith, M. D.; Connor, B. A.; Karunadasa, H. I. Tuning the Luminescence of Layered Halide Perovskites. *Chem. Rev.* **2019**, *119*, 3104−3139.
(51) Mao, L.; Stoumpos, C. C.; Kanatzidis, M. G. Two-Dimensional Hybrid Halide Perovskites: Principles and Promises. *J. Am. Chem. Soc.* **2019**, *141*, 1171−1190.
(52) Cao, D. H.; Stoumpos, C. C.; Yokoyama, T.; Logsdon, J. L.; Song, T.-B.; Farha, O. K.; Wasielewski, M. R.; Hupp, J. T.; Kanatzidis, M. G. Thin Films and Solar Cells Based on Semiconducting Two-Dimensional Ruddlesden−Popper $(CH_3(CH_2)_3NH_3)_2(CH_3NH_3)_{n-1}Sn_nI_{3n+1}$ Perovskites. *ACS Energy Lett.* **2017**, *2*, 982−990.
(53) Tsai, H.; Nie, W.; Blancon, J.-C.; Stoumpos, C. C.; Asadpour, R.; Harutyunyan, B.; Neukirch, A. J.; Verduzco, R.; Crochet, J. J.; Tretiak, S.; Pedesseau, L.; Even, J.; Alam, M. A.; Gupta, G.; Lou, J.; Ajayan, P. M.; Bedzyk, M. J.; Kanatzidis, M. G.; Mohite, A. D. High-efficiency two-dimensional Ruddlesden−Popper perovskite solar cells. *Nature* **2016**, *536*, 312−316.
(54) Yaffe, O.; Chernikov, A.; Norman, Z. M.; Zhong, Y.; Velauthapillai, A.; van der Zande, A.; Owen, J. S.; Heinz, T. F. Excitons in ultrathin organic−inorganic perovskite crystals. *Phys. Rev. B: Condens. Matter Mater. Phys.* **2015**, *92*, 045414.
(55) Mitzi, D. B.; Wang, S.; Feild, C. A.; Chess, C. A.; Guloy, A. M. Conducting Layered Organic−Inorganic Halides Containing ⟨110⟩-Oriented Perovskite Sheets. *Science* **1995**, *267*, 1473.
(56) Li, X.; Guo, P.; Kepenekian, M.; Hadar, I.; Katan, C.; Even, J.; Stoumpos, C. C.; Schaller, R. D.; Kanatzidis, M. G. Small Cyclic Diammonium Cation Templated (110)-Oriented 2D Halide (X = I, Br, Cl) Perovskites with White-Light Emission. *Chem. Mater.* **2019**, *31*, 3582−3590.
(57) Hu, T.; Smith, M. D.; Dohner, E. R.; Sher, M.-J.; Wu, X.; Trinh, M. T.; Fisher, A.; Corbett, J.; Zhu, X. Y.; Karunadasa, H. I.; Lindenberg, A. M. Mechanism for Broadband White-Light Emission from Two-Dimensional (110) Hybrid Perovskites. *J. Phys. Chem. Lett.* **2016**, *7*, 2258−2263.
(58) Cortecchia, D.; Yin, J.; Bruno, A.; Lo, S.-Z. A.; Gurzadyan, G. G.; Mhaisalkar, S.; Bredas, J.-L.; Soci, C. Polaron self-localization in white-light emitting hybrid perovskites. *J. Mater. Chem. C* **2017**, *5*, 2771−2780.
(59) McCall, K. M.; Stoumpos, C. C.; Kostina, S. S.; Kanatzidis, M. G.; Wessels, B. W. Strong Electron−Phonon Coupling and Self-Trapped Excitons in the Defect Halide Perovskites $A_3M_2I_9$ (A = Cs, Rb; M = Bi, Sb). *Chem. Mater.* **2017**, *29*, 4129−4145.
(60) Chang, J.-H.; Doert, T.; Ruck, M. Structural Variety of Defect Perovskite Variants $M_3E_2X_9$ (M = Rb, Tl, E = Bi, Sb, X = Br, I). *Z. Anorg. Allg. Chem.* **2016**, *642*, 736−748.
(61) McCall, K. M.; Liu, Z.; Trimarchi, G.; Stoumpos, C. C.; Lin, W.; He, Y.; Hadar, I.; Kanatzidis, M. G.; Wessels, B. W. α-Particle Detection and Charge Transport Characteristics in the $A_3M_2I_9$ Defect Perovskites (A = Cs, Rb; M = Bi, Sb). *ACS Photonics* **2018**, *5*, 3748−3762.
(62) McCall, K. M.; Stoumpos, C. C.; Kontsevoi, O. Y.; Alexander, G. C. B.; Wessels, B. W.; Kanatzidis, M. G. From 0D $Cs_3Bi_2I_9$ to 2D $Cs_3Bi_2I_6Cl_3$: Dimensional Expansion Induces a Direct Band Gap but Enhances Electron−Phonon Coupling. *Chem. Mater.* **2019**, *31*, 2644−2650.
(63) Jakubas, R.; Gągor, A.; Winiarski, M. J.; Ptak, M.; Piecha-Bisiorek, A.; Ciżman, A. Ferroelectricity in Ethylammonium Bismuth-Based Organic−Inorganic Hybrid: $(C_2H_5NH_3)_2[BiBr_5]$. *Inorg. Chem.* **2020**, *59*, 3417−3427.
(64) Kelly, A. W.; Nicholas, A.; Ahern, J. C.; Chan, B.; Patterson, H. H.; Pike, R. D. Alkali metal bismuth(III) chloride double salts. *J. Alloys Compd.* **2016**, *670*, 337−345.
(65) Timmermans, C. W. M.; Cholakh, S. O.; Blasse, G. The luminescence of $Cs_3Bi_2Cl_9$ and $Cs_3Sb_2Cl_9$. *J. Solid State Chem.* **1983**, *46*, 222−233.
(66) Yuan, Z.; Zhou, C.; Tian, Y.; Shu, Y.; Messier, J.; Wang, J. C.; van de Burgt, L. J.; Kountouriotis, K.; Xin, Y.; Holt, E.; Schanze, K.; Clark, R.; Siegrist, T.; Ma, B. One-dimensional organic lead halide perovskites with efficient bluish white-light emission. *Nat. Commun.* **2017**, *8*, 14051.
(67) Jakubas, R.; Rok, M.; Mencel, K.; Bator, G.; Piecha-Bisiorek, A. Correlation between crystal structure and polar (ferroelectric) properties of haloantimonates(III) and halobismuthates(III) hybrids. *Inorg. Chem. Front.* **2020**, *7*, 2107−2128.
(68) Bujak, M.; Zaleski, J. Synthesis and structure of tetrakis-(tetramethylammonium) octacosachlorooctaantimonate(III) $[(CH_3)_4N]_4Sb_8Cl_{28}$. *J. Mol. Struct.* **2000**, *555*, 179−185.
(69) Mercier, N.; Louvain, N.; Bi, W. Structural diversity and retro-crystal engineering analysis of iodometalate hybrids. *CrystEngComm* **2009**, *11*, 720−734.
(70) Beck, H. P.; Clicqué, G.; Nau, H. A Study on AB_2X_5 Compounds (A: K, In, Tl; B: Sr, Sn, Pb; X: Cl, Br, I). *Z. Anorg. Allg. Chem.* **1986**, *536*, 35−44.
(71) Liu, X.; Wu, W.; Zhang, Y.; Li, Y.; Wu, H.; Fan, J. Critical Roles of High- and Low-Frequency Optical Phonons in Photodynamics of Zero-Dimensional Perovskite-like $(C_6H_{22}N_4Cl_3)SnCl_3$ Crystals. *J. Phys. Chem. Lett.* **2019**, *10*, 7586−7593.
(72) Chen, F.; Wang, S.; Li, Y.-H.; Huang, W. Effects of Anionic Geometries on Hydrogen-Bonding Networks of 1-(4-pyridyl) Piperazine. *J. Chem. Crystallogr.* **2016**, *46*, 309−323.
(73) Mitzi, D. B.; Feild, C. A.; Harrison, W. T. A.; Guloy, A. M. Conducting tin halides with a layered organic-based perovskite structure. *Nature* **1994**, *369*, 467−469.
(74) Wojciechowska, M.; Szklarz, P.; Białońska, A.; Baran, J.; Janicki, R.; Medycki, W.; Durlak, P.; Piecha-Bisiorek, A.; Jakubas, R. Enormous lattice distortion through an isomorphous phase transition in an organic−inorganic hybrid based on haloantimonate(III). *CrystEngComm* **2016**, *18*, 6184−6194.
(75) Hashimoto, M.; Hashimoto, S.; Terao, H.; Kuma, M.; Niki, H.; Ino, H. Crystal Structure and Phase Transition of 4-Aminopyridinium Tetrabromoantimonate(III) as Studied by Bromine and Antimony NQR, Proton NMR, and Single Crystal X-Ray Diffraction. *Z. Naturforsch., A: Phys. Sci.* **2000**, *55*, 167−172.
(76) McNulty, J. A.; Lightfoot, P. Unprecedented tin iodide perovskite-like structures featuring ordering of organic moieties. *Chem. Commun.* **2020**, *56*, 4543−4546.
(77) Reich, O.; Hasche, S.; Bonmann, S.; Krebs, B. $[H_3O\cdot(Dibenzo\text{-}18\text{-}crown\text{-}6)][Te_2Br_9]$ and $[H_5O_2][Te_2Cl_9]\cdot 2C_4H_8O_2$: Two New Oxonium Halotellurates(IV) Containing a Novel Type of $[Te_2X_9]^-$ Anions. *Z. Anorg. Allg. Chem.* **1998**, *624*, 411−418.
(78) Stöwe, K.; Beck, H. P. Low temperature polymorphs of the compound In_3SnI_5. *Z. Kristallogr. - Cryst. Mater.* **1994**, *209*, 36−42.

https://dx.doi.org/10.1021/acsmaterialslett.0c00211
ACS Materials Lett. 2020, 2, 1218−1232

(79) Benin, B. M.; McCall, K. M.; Woerle, M.; Morad, V.; Aebli, M.; Yakunin, S.; Shynkarenko, Y.; Kovalenko, M. V. The $Rb_7Bi_{3-3x}Sb_{3x}Cl_{16}$ family: A Fully Inorganic Solid Solution with Room-Temperature Luminescent Members. *Angew. Chem., Int. Ed.* **2020**, *59*, 14490−14497.
(80) Krebs, B.; Büscher, K. Dimere Halogenotellurate(IV): Darstellung und Kristallstruktur von $[(C_6H_5)_4P]_2Te_2Br_{10}$. *Z. Anorg. Allg. Chem.* **1980**, *463*, 56−64.
(81) Wang, S.; Mitzi, D. B.; Feild, C. A.; Guloy, A. Synthesis and Characterization of $[NH_2C(I){=}NH_2]_3MI_5$ (M = Sn, Pb): Stereochemical Activity in Divalent Tin and Lead Halides Containing Single ⟨110⟩ Perovskite Sheets. *J. Am. Chem. Soc.* **1995**, *117*, 5297−5302.
(82) Ksiądzyna, M.; Gągor, A.; Piecha-Bisiorek, A.; Ciżman, A.; Medycki, W.; Jakubas, R. Exploring a hybrid ferroelectric with a 1-D perovskite-like structure: bis(pyrrolidinium) pentachloroantimonate-(III). *J. Mater. Chem. C* **2019**, *7*, 10360−10370.
(83) Krebs, B.; Buss, B.; Berger, W. Kristall- und Molekülstruktur von $TeCl_4{\cdot}PCl_5$ ($=PCl_4^+TeCl_5^-$). Der stereochemische Einfluß des inerten Elektronenpaars in Tellur(IV)-chlorverbindungen. *Z. Anorg. Allg. Chem.* **1973**, *397*, 1−15.
(84) Piecha, A.; Pietraszko, A.; Bator, G.; Jakubas, R. Structural characterization and ferroelectric ordering in $(C_3N_2H_5)_5Sb_2Br_{11}$. *J. Solid State Chem.* **2008**, *181*, 1155−1166.
(85) Wang, Z.; Zhang, Z.; Tao, L.; Shen, N.; Hu, B.; Gong, L.; Li, J.; Chen, X.; Huang, X.-Y. Hybrid Chloroantimonates(III): Thermally Induced Triple-Mode Reversible Luminescent Switching and Laser-Printable Rewritable Luminescent Paper. *Angew. Chem., Int. Ed.* **2019**, *58*, 9974−9978.
(86) Blasse, G.; Dirksen, G. J.; Abriel, W. The influence of distortion of the Te(IV) coordination octahedron on its luminescence. *Chem. Phys. Lett.* **1987**, *136*, 460−464.
(87) Krebs, B.; Ahlers, F.-P. Developments in Chalcogen−Halide Chemistry. *Adv. Inorg. Chem.* **1990**, *35*, 235−317.
(88) Stufkens, D. J. Dynamic Jahn−Teller effect in the excited states of $SeCl_6^{2-}$, $SeBr_6^{2-}$, $TeCl_6^{2-}$ and $TeBr_6^{2-}$: Interpretation of electronic absorption and Raman spectra. *Recl. Trav. Chim. Pays-Bas* **1970**, *89*, 1185−1201.
(89) Chen, D.; Dai, F.; Hao, S.; Zhou, G.; Liu, Q.; Wolverton, C. M.; Zhao, J.; Xia, Z. Crystal Structure and Luminescence Properties of Lead-Free Metal Halides: $(C_6H_5CH_2NH_3)_3MBr_6$ (M = Bi and Sb). *J. Mater. Chem. C* **2020**, *8*, 7322−7329.
(90) Clark, R. J. H.; Stead, M. J. Raman spectroscopy of the $[TeX_6]^{2-}$ ions (X = Cl or Br) at resonance with their lowest $^3T_{1u}$ and $^1T_{1u}$ states: Evidence for tetragonal distortion in these excited states. *Chem. Phys.* **1984**, *91*, 113−118.
(91) Degen, J.; Schmidtke, H. H.; Chatzidimitriou-Dreismann, C. A. Observation of dynamically induced fluctuations of the photon flux and resolution of the broad luminescence band of Cs_2TeBr_6. *Theoretica chimica acta* **1985**, *67*, 37−42.
(92) Shi, H.; Han, D.; Chen, S.; Du, M.-H. Impact of metal ns^2 lone pair on luminescence quantum efficiency in low-dimensional halide perovskites. *Phys. Rev. Mater.* **2019**, *3*, 034604.
(93) Sidgwick, N. V. *The Covalent Link in Chemistry*; Cornell University Press: Ithaca, NY, 1933.
(94) Pyykko, P. Relativistic effects in structural chemistry. *Chem. Rev.* **1988**, *88*, 563−594.
(95) Stoumpos, C. C.; Frazer, L.; Clark, D. J.; Kim, Y. S.; Rhim, S. H.; Freeman, A. J.; Ketterson, J. B.; Jang, J. I.; Kanatzidis, M. G. Hybrid Germanium Iodide Perovskite Semiconductors: Active Lone Pairs, Structural Distortions, Direct and Indirect Energy Gaps, and Strong Nonlinear Optical Properties. *J. Am. Chem. Soc.* **2015**, *137*, 6804−6819.
(96) Swainson, I.; Chi, L.; Her, J.-H.; Cranswick, L.; Stephens, P.; Winkler, B.; Wilson, D. J.; Milman, V. Orientational ordering, tilting and lone-pair activity in the perovskite methylammonium tin bromide, $CH_3NH_3SnBr_3$. *Acta Crystallogr., Sect. B: Struct. Sci.* **2010**, *66*, 422−429.
(97) Schueller, E. C.; Laurita, G.; Fabini, D. H.; Stoumpos, C. C.; Kanatzidis, M. G.; Seshadri, R. Crystal Structure Evolution and Notable Thermal Expansion in Hybrid Perovskites Formamidinium Tin Iodide and Formamidinium Lead Bromide. *Inorg. Chem.* **2018**, *57*, 695−701.
(98) Fabini, D. H.; Laurita, G.; Bechtel, J. S.; Stoumpos, C. C.; Evans, H. A.; Kontos, A. G.; Raptis, Y. S.; Falaras, P.; Van der Ven, A.; Kanatzidis, M. G.; Seshadri, R. Dynamic Stereochemical Activity of the Sn^{2+} Lone Pair in Perovskite $CsSnBr_3$. *J. Am. Chem. Soc.* **2016**, *138*, 11820−32.
(99) Laurita, G.; Fabini, D. H.; Stoumpos, C. C.; Kanatzidis, M. G.; Seshadri, R. Chemical tuning of dynamic cation off-centering in the cubic phases of hybrid tin and lead halide perovskites. *Chem. Sci.* **2017**, *8*, 5628−5635.
(100) Abrahams, I.; Demetriou, D. Z. Inert Pair Effects in Tin and Lead Dihalides: Crystal Structure of Tin(II) Bromide. *J. Solid State Chem.* **2000**, *149*, 28−32.
(101) Wheeler, R. A.; Kumar, P. N. V. P. Stereochemically active or inactive lone pair electrons in some six-coordinate, group 15 halides. *J. Am. Chem. Soc.* **1992**, *114*, 4776−4784.
(102) Morss, L. R.; Siegal, M.; Stenger, L.; Edelstein, N. Preparation of cubic chloro complex compounds of trivalent metals: Cs_2NaMCl_6. *Inorg. Chem.* **1970**, *9*, 1771−1775.
(103) Shannon, R. Revised effective ionic radii and systematic studies of interatomic distances in halides and chalcogenides. *Acta Crystallogr., Sect. A: Cryst. Phys., Diffr., Theor. Gen. Crystallogr.* **1976**, *32*, 751−767.
(104) Akkerman, Q. A.; Park, S.; Radicchi, E.; Nunzi, F.; Mosconi, E.; De Angelis, F.; Brescia, R.; Rastogi, P.; Prato, M.; Manna, L. Nearly Monodisperse Insulator Cs_4PbX_6 (X = Cl, Br, I) Nanocrystals, Their Mixed Halide Compositions, and Their Transformation into $CsPbX_3$ Nanocrystals. *Nano Lett.* **2017**, *17*, 1924−1930.
(105) Qin, Z. J.; Dai, S. Y.; Hadjiev, V. G.; Wang, C.; Xie, L. X.; Ni, Y. Z.; Wu, C. Z.; Yang, G.; Chen, S.; Deng, L. Z.; Yu, Q. K.; Feng, G. Y.; Wang, Z. M. M.; Bao, J. M. Revealing the Origin of Luminescence Center in 0D Cs_4PbBr_6 Perovskite. *Chem. Mater.* **2019**, *31*, 9098−9104.
(106) Xu, J.; Li, S.; Qin, C.; Feng, Z.; Du, Y. Identification of Singlet Self-Trapped Excitons in a New Family of White-Light-Emitting Zero-Dimensional Compounds. *J. Phys. Chem. C* **2020**, *124*, 11625−11630.
(107) Jing, Y.; Liu, Y.; Jiang, X.; Molokeev, M. S.; Lin, Z.; Xia, Z. Sb^{3+} Dopant and Halogen Substitution Triggered Highly Efficient and Tunable Emission in Lead-Free Metal Halide Single Crystals. *Chem. Mater.* **2020**, *32*, 5327−5334.
(108) Blasse, G.; Grabmaier, B. C. *Luminescent Materials*; Springer: Berlin, 1994.
(109) Jacobs, P. W. M. Alkali halide crystals containing impurity ions with the ns^2 ground-state electronic configuration. *J. Phys. Chem. Solids* **1991**, *52*, 35−67.
(110) Pelant, I.; Valenta, J. *Luminescence Spectroscopy of Semiconductors*; Oxford University Press: New York, 2012.
(111) Luo, J.; Wang, X.; Li, S.; Liu, J.; Guo, Y.; Niu, G.; Yao, L.; Fu, Y.; Gao, L.; Dong, Q.; Zhao, C.; Leng, M.; Ma, F.; Liang, W.; Wang, L.; Jin, S.; Han, J.; Zhang, L.; Etheridge, J.; Wang, J.; Yan, Y.; Sargent, E. H.; Tang, J. Efficient and stable emission of warm-white light from lead-free halide double perovskites. *Nature* **2018**, *563*, 541−545.
(112) Li, S.; Luo, J.; Liu, J.; Tang, J. Self-Trapped Excitons in All-Inorganic Halide Perovskites: Fundamentals, Status, and Potential Applications. *J. Phys. Chem. Lett.* **2019**, *10*, 1999−2007.
(113) Sedakova, T. V.; Mirochnik, A. G.; Karasev, V. E. Structure and luminescence properties of tellurium(IV) complex compounds. *Opt. Spectrosc.* **2011**, *110*, 755.
(114) Sedakova, T. V.; Mirochnik, A. G. Luminescent and thermochromic properties of tellurium(IV) halide complexes with cesium. *Opt. Spectrosc.* **2016**, *120*, 268−273.
(115) Dotsenko, A. A.; Vovna, V. I.; Korochentsev, V. V.; Mirochnik, A. G.; Shcheka, O. L.; Sedakova, T. V.; Sergienko, V. I. Halide Perovskite-Derived Compounds Rb_2TeX_6 (X = Cl, Br, and I): Electronic Structure of the Ground and First Excited States. *Inorg. Chem.* **2019**, *58*, 6796−6803.
(116) Li, J.; Stoumpos, C. C.; Trimarchi, G. G.; Chung, I.; Mao, L.; Chen, M.; Wasielewski, M. R.; Wang, L.; Kanatzidis, M. G. Air-Stable Direct Bandgap Perovskite Semiconductors: All-Inorganic Tin-Based Heteroleptic Halides $A_xSnCl_yI_z$ (A = Cs, Rb). *Chem. Mater.* **2018**, *30*, 4847−4856.

https://dx.doi.org/10.1021/acsmaterialslett.0c00211
ACS Materials Lett. 2020, 2, 1218−1232

(117) Donaldson, J. D.; Grimes, S. M. The inorganic chemistry of tin. In *Chemistry of Tin*; Smith, P. J., Ed.; Springer: Dordrecht, The Netherlands, 1998; pp 62−94.
(118) Morad, V.; Yakunin, S.; Kovalenko, M. V. Supramolecular Approach for Fine-Tuning of the Bright Luminescence from Zero-Dimensional Antimony(III) Halides. *ACS Mater. Lett.* **2020**, *2*, 845−852.
(119) He, Q.; Zhou, C.; Xu, L.; Lee, S.; Lin, X.; Neu, J.; Worku, M.; Chaaban, M.; Ma, B. Highly Stable Organic Antimony Halide Crystals for X-ray Scintillation. *ACS Mater. Lett.* **2020**, *2*, 633−638.
(120) Fu, P.; Huang, M.; Shang, Y.; Yu, N.; Zhou, H.-L.; Zhang, Y.-B.; Chen, S.; Gong, J.; Ning, Z. Organic−Inorganic Layered and Hollow Tin Bromide Perovskite with Tunable Broadband Emission. *ACS Appl. Mater. Interfaces* **2018**, *10*, 34363−34369.
(121) Xu, L.-J.; Lin, H.; Lee, S.; Zhou, C.; Worku, M.; Chaaban, M.; He, Q.; Plaviak, A.; Lin, X.; Chen, B.; Du, M.-H.; Ma, B. 0D and 2D: The Cases of Phenylethylammonium Tin Bromide Hybrids. *Chem. Mater.* **2020**, *32*, 4692−4698.
(122) Zhou, C.; Worku, M.; Neu, J.; Lin, H.; Tian, Y.; Lee, S.; Zhou, Y.; Han, D.; Chen, S.; Hao, A.; Djurovich, P. I.; Siegrist, T.; Du, M.-H.; Ma, B. Facile Preparation of Light Emitting Organic Metal Halide Crystals with Near-Unity Quantum Efficiency. *Chem. Mater.* **2018**, *30*, 2374−2378.
(123) Chabot, B.; Parthe, E. $Cs_3Sb_2I_9$ and $Cs_3Bi_2I_9$ with the hexagonal $Cs_3Cr_2Cl_9$ structure type. *Acta Crystallogr., Sect. B: Struct. Crystallogr. Cryst. Chem.* **1978**, *34*, 645−648.
(124) Zhou, C.; Lin, H.; Neu, J.; Zhou, Y.; Chaaban, M.; Lee, S.; Worku, M.; Chen, B.; Clark, R.; Cheng, W.; Guan, J.; Djurovich, P.; Zhang, D.; Lü, X.; Bullock, J.; Pak, C.; Shatruk, M.; Du, M.-H.; Siegrist, T.; Ma, B. Green Emitting Single-Crystalline Bulk Assembly of Metal Halide Clusters with Near-Unity Photoluminescence Quantum Efficiency. *ACS Energy Lett.* **2019**, *4*, 1579−1583.
(125) Ueta, M.; Kanzaki, H.; Kobayashi, K.; Toyozawa, Y.; Hanamura, E. Exciton−Phonon Processes in Silver Halides. In *Excitonic Processes in Solids*; Ueta, M., Kanzaki, H., Kobayashi, K., Toyozawa, Y., Hanamura, E., Eds.; Springer: Berlin, 1986; pp 309−369.
(126) Song, K. S.; Williams, R. T. Silver Halides. In *Self-Trapped Excitons*; Song, K. S., Williams, R. T., Eds.; Springer: Berlin, 1993; pp 319−338.
(127) Edamatsu, K.; Ikezawa, M.; Tokailin, H.; Takahashi, T.; Sagawa, T. Energy Band Structure and Fundamental Optical Absorption of Alkali Cuprous Halide and Alkali Silver Halide Crystals. *J. Phys. Soc. Jpn.* **1986**, *55*, 2880−2888.
(128) Jun, T.; Sim, K.; Iimura, S.; Sasase, M.; Kamioka, H.; Kim, J.; Hosono, H. Lead-Free Highly Efficient Blue-Emitting $Cs_3Cu_2I_5$ with 0D Electronic Structure. *Adv. Mater.* **2018**, *30*, 1804547.
(129) Lian, L.; Zheng, M.; Zhang, W.; Yin, L.; Du, X.; Zhang, P.; Zhang, X.; Gao, J.; Zhang, D.; Gao, L.; Niu, G.; Song, H.; Chen, R.; Lan, X.; Tang, J.; Zhang, J. Efficient and Reabsorption-Free Radioluminescence in $Cs_3Cu_2I_5$ Nanocrystals with Self-Trapped Excitons. *Adv. Sci.* **2020**, *7*, 2000195.
(130) Zhao, X.; Niu, G.; Zhu, J.; Yang, B.; Yuan, J.-H.; Li, S.; Gao, W.; Hu, Q.; Yin, L.; Xue, K.-H.; Lifshitz, E.; Miao, X.; Tang, J. All-Inorganic Copper Halide as a Stable and Self-Absorption-Free X-ray Scintillator. *J. Phys. Chem. Lett.* **2020**, *11*, 1873−1880.
(131) Olaru, M.; Rychagova, E.; Ketkov, S.; Shynkarenko, Y.; Yakunin, S.; Kovalenko, M. V.; Yablonskiy, A.; Andreev, B.; Kleemiss, F.; Beckmann, J.; Vogt, M. A Small Cationic Organo−Copper Cluster as Thermally Robust Highly Photo- and Electroluminescent Material. *J. Am. Chem. Soc.* **2020**, *142*, 373−381.
(132) Gautier, R.; Paris, M.; Massuyeau, F. Hydrogen Bonding and Broad-Band Emission in Hybrid Zinc Halide Phosphors. *Inorg. Chem.* **2020**, *59*, 2626−2630.
(133) Zhang, X.; Li, L.; Wang, S.; Liu, X.; Yao, Y.; Peng, Y.; Hong, M.; Luo, J. [(N-AEPz)$ZnCl_4$]Cl: A "Green" Metal Halide Showing Highly Efficient Bluish-White-Light Emission. *Inorg. Chem.* **2020**, *59*, 3527−3531.
(134) Roccanova, R.; Ming, W.; Whiteside, V. R.; McGuire, M. A.; Sellers, I. R.; Du, M.-H.; Saparov, B. Synthesis, Crystal and Electronic Structures, and Optical Properties of $(CH_3NH_3)_2CdX_4$ (X = Cl, Br, I). *Inorg. Chem.* **2017**, *56*, 13878−13888.
(135) Li, X.; Wang, S.; Zhao, S.; Li, L.; Li, Y.; Zhao, B.; Shen, Y.; Wu, Z.; Shan, P.; Luo, J. Mixing Halogens To Assemble an All-Inorganic Layered Perovskite with Warm White-Light Emission. *Chem. - Eur. J.* **2018**, *24*, 9243−9246.
(136) Luo, B.; Liang, D.; Sun, S.; Xiao, Y.; Lian, X.; Li, X.; Li, M.-D.; Huang, X.-C.; Zhang, J. Z. Breaking Forbidden Transitions for Emission of Self-Trapped Excitons in Two Dimensional $(F_2CHCH_2NH_3)_2CdBr_4$ Perovskite through Pb Alloying. *J. Phys. Chem. Lett.* **2020**, *11*, 199−205.
(137) Zhou, L.; Liao, J.-F.; Huang, Z.-G.; Wei, J.-H.; Wang, X.-D.; Chen, H.-Y.; Kuang, D.-B. Intrinsic Self-Trapped Emission in 0D Lead-Free $(C_4H_{14}N_2)_2In_2Br_{10}$ Single Crystal. *Angew. Chem., Int. Ed.* **2019**, *58*, 15435−15440.
(138) Zhou, L.; Liao, J.-F.; Huang, Z.-G.; Wei, J.-H.; Wang, X.-D.; Li, W.-G.; Chen, H.-Y.; Kuang, D.-B.; Su, C.-Y. Highly Red Emissive Lead-Free Indium-Based Perovskite Single Crystal for Sensitive Water Detection. *Angew. Chem., Int. Ed.* **2019**, *58*, 5277−5281.
(139) Zeng, R.; Zhang, L.; Xue, Y.; Ke, B.; Zhao, Z.; Huang, D.; Wei, Q.; Zhou, W.; Zou, B. Highly Efficient Blue Emission from Self-Trapped Excitons in Stable Sb3+-Doped Cs2NaInCl6 Double Perovskites. *J. Phys. Chem. Lett.* **2020**, *11*, 2053−2061.
(140) Noculak, A.; Morad, V.; McCall, K. M.; Yakunin, S.; Shynkarenko, Y.; Wörle, M.; Kovalenko, M. V. Bright Blue and Green Luminescence of Sb(III) in Double Perovskite Cs_2MInCl_6 (M = Na, K) Matrices. *Chem. Mater.* **2020**, *32*, 5118−5124.
(141) Li, T.; Chen, X.; Wang, X.; Lu, H.; Yan, Y.; Beard, M. C.; Mitzi, D. B. Origin of Broad-Band Emission and Impact of Structural Dimensionality in Tin-Alloyed Ruddlesden−Popper Hybrid Lead Iodide Perovskites. *ACS Energy Lett.* **2020**, *5*, 347−352.
(142) Kentsch, R.; Scholz, M.; Horn, J.; Schlettwein, D.; Oum, K.; Lenzer, T. Exciton Dynamics and Electron−Phonon Coupling Affect the Photovoltaic Performance of the $Cs_2AgBiBr_6$ Double Perovskite. *J. Phys. Chem. C* **2018**, *122*, 25940−25947.
(143) Liu, C.; Wang, Y.; Geng, h.; Zhu, T.; Ertekin, E.; Gosztola, D. J.; Yang, S.; Huang, J.; Yang, B.; Han, K.; Canton, S. E.; Kong, Q.; Zheng, K.; Zhang, X. Asynchronous Photoexcited Electronic and Structural Relaxation in Lead Free Perovskites. *J. Am. Chem. Soc.* **2019**, *141*, 13074−13080.
(144) Wu, X.; Tan, L. Z.; Shen, X.; Hu, T.; Miyata, K.; Trinh, M. T.; Li, R.; Coffee, R.; Liu, S.; Egger, D. A.; Makasyuk, I.; Zheng, Q.; Fry, A.; Robinson, J. S.; Smith, M. D.; Guzelturk, B.; Karunadasa, H. I.; Wang, X.; Zhu, X.; Kronik, L.; Rappe, A. M.; Lindenberg, A. M. Light-induced picosecond rotational disordering of the inorganic sublattice in hybrid perovskites. *Sci. Adv.* **2017**, *3*, e1602388.
(145) Chiara, R.; Ciftci, Y. O.; Queloz, V. I. E.; Nazeeruddin, M. K.; Grancini, G.; Malavasi, L. Green-Emitting Lead-Free Cs_4SnBr_6 Zero-Dimensional Perovskite Nanocrystals with Improved Air Stability. *J. Phys. Chem. Lett.* **2020**, *11*, 618−623.
(146) Tan, L.; Wang, W.; Li, Q.; Luo, Z.; Zou, C.; Tang, M.; Zhang, L.; He, J.; Quan, Z. Colloidal syntheses of zero-dimensional Cs_4SnX_6 (X = Br, I) nanocrystals with high emission efficiencies. *Chem. Commun.* **2020**, *56*, 387−390.
(147) Yang, T.-H.; Huang, H.-Y.; Sun, C.-C.; Glorieux, B.; Lee, X.-H.; Yu, Y.-W.; Chung, T.-Y. Noncontact and instant detection of phosphor temperature in phosphor-converted white LEDs. *Sci. Rep.* **2018**, *8*, 296.
(148) Bachmann, V.; Ronda, C.; Meijerink, A. Temperature Quenching of Yellow Ce^{3+} Luminescence in YAG:Ce. *Chem. Mater.* **2009**, *21*, 2077−2084.
(149) Worku, M.; Tian, Y.; Zhou, C.; Lee, S.; Meisner, Q.; Zhou, Y.; Ma, B. Sunlike White-Light-Emitting Diodes Based on Zero-Dimensional Organic Metal Halide Hybrids. *ACS Appl. Mater. Interfaces* **2018**, *10*, 30051−30057.

https://dx.doi.org/10.1021/acsmaterialslett.0c00211
ACS Materials Lett. 2020, 2, 1218−1232